NASA Contractor Report 172596

NASA-CR-172596
19850019155

VALIDATION OF THE ERBE SCANNER SCENE IDENTIFICATION METHODOLOGY: ANALYSIS WITH NIMBUS-7 ERB DATA

Sastri Vermury

S M SYSTEMS AND RESEARCH CORPORATION
Landover, Maryland

Purchase Order L-67978B
March 1985

National Aeronautics and
Space Administration

Langley Research Center
Hampton, Virginia 23665

Table of Contents

1. INTRODUCTION:

Estimation of fluxes from satellite radiance measurements is known to be sensitive to the models used in the conversion and to the proper identification of the scene (Ruff et al., 1968; Raschke et al., 1973) particularly cloud. The models used in the radiance to flux conversion are the bidirectional and directional models for clear and cloudy (with different levels of cloudiness) scenes. The cloud identification for this purpose is derived from the narrow band 11.5 μm channel on the Temperature Humidity Infrared Radiometer (THIR) on Nimbus-7 (Chen et al., 1980; Hwang, 1982). The scene identification in the data processing stream for Nimbus-7 Earth Radiation Budget (ERB) instrument is based on bispectral thresholds (Jacobowitz et al., 1984) on the broad band radiance measurements in the short wave (0.2 to 4.8 μm) and the long wave (4.5 μm to 50 μm). Scene determination using thresholding methods is shown to be deficient and some alternatives were suggested in Vemury et al. (1984). Data from the Earth Radiation Budget Experiment (ERBE) will be processed using a statistical procedure known as the Maximum Likelihood Estimation (MLE), for detection of cloud amount using the SW and LW radiance measurements.

This scene information derived from NFOV channels is also used in the inversion process for the medium field of view and wide field of view (MFOV and WFOV) channels on the ERBE instrument. Correct scene identification from the narrow field of view (NFOV) channels, is thus of great importance.

This report is based upon a study to test the MLE procedure and evalute its performance on actually observed radiance data from the narrow field of view (NFOV) channels on the Nimbus-7 ERB instrument. The Earth radiation budget parameters obtained with the MLE procedure will be compared with those obtained from the Sorting into Angular Bins (SAB) method. The present study also serves as a test of performance of the scene identification algorithm to be used in the ERBE data stream.

2. Description of SAB and MLE Methods:

Since scene selection is an identified problem with most inversion methods, the results obtained with the MLE method will be validated by using a data set which is independent of scene identification and corresponding scene dependent bidirectional models. Sorting into Angular Bins (SAB) method provides such a validation data set. (For details see Arking et al., 1984). This method essentially involves the binning of the SW and LW radiance measurements into different solid angle bins (85 in all) for each equal surface area region on the globe referred to as a target area (TA). One month of data is sorted into these bins to provide adequate sample size in each of the 85 bins for each TA. The radiance means for each bin for the month are computed and for each TA, the 85 bin radiance means are integrated with the appropriate solid angle weight for the bin to obtain the TA flux. This process involves no scene identification and is really independent of the underlying scene, viz., cloud or no cloud and also of the associated angular models.

A directional model is necessary to obtain a mean daily albedo from the instantaneous albedo for the TA. In the present study, mean daily albedos are not calculated in order to reduce the complexity of the problem. All the albedos referred to in the study are instantaneous albedos.

The input data set for this method is the Sub-target Radiance Tape (STRT) which contains 9 days of data compacted into one tape. Some necessary definitions are given in Frame 1 and Frame 2 and a very brief description of the SAB procedure is shown in Frame 3. On the same frame, a few comments are made on the data quality checks and processing methods.

The binning procedure will fail if the sample sizes for the bins are not adequate so that one is required to fill a number of bins with interpolation for the TAs. The number of TAs rejected due to lack of adequate sample sizes is found to be rather small in all cases, viz., reflected radiances, emitted day time and emitted night time radiances. Figures 1 and 2 show this result schematically on a latitude band basis. The abscissa is the zone number, 1 for the South Pole and 40 for the North Pole; each latitude band is 4.5° wide. At each latitude, the number of TAs rejected is shown by the dashed line while the solid line indicates the total number of TAs in that band. It is obvious that a very small number of TAs are being rejected with the binning process.

The SAB algorithm consists of software at three levels. At Level I, the radiance observations are grouped into TAs and for each TA, into angular bins and radiances and sample sizes are accumulated for all the days in the month. The Level II algo-

rithm uses the output from Level I stored on tape and after quality control checks, fills any empty bins and for each TA, if accepted, integrates the radiance means over the solid angles to obtain the flux. Output products for Level II are the reflected and emitted fluxes (day and night) for each TA with a few subsidiary pieces of information. Level III software computes the zonally, and globally averaged earth radiation budget parameters.

Maximum Likelihood Estimation:

The input data set for this method is the Master Archival Tape (MAT) which consists of corrected earth located radiance values. There is one MAT tape for day. The other input is the table of anisotropic factors (reflectance and emission) for each of 12 earth scenes identified for use by ERBE algorithm. A brief description of the MLE procedure is given in Frames 4 and 5. No further details about the MLE method will be discussed since the ERBE team is quite familiar with most of the details.

3. Operational Steps

The following sequential steps were performed to retain the integrity of the original MATRIX algorithm, while the modifications were made.

(i) The MATRIX algorithms were modified to be able to process the NFOV data only on a daily basis. The results of a few days of data were compared with MATRIX output.

(ii) The code was further modified to compute the instantaneous albedoes only. No directional

models were used in the present study.

(iii)(a) The MLE scene identification algorithm was set up for latitude, longitude directions different from those accepted by Nimbus-7 ERB MATRIX algorithms. Also, the spatial resolution and global grid structure used by the MLE system are different. Therefore the Scene ID was performed on the ERBE grid structure, but the derived fluxes were stored for the MATRIX TA grid. This is necessary to make the comparison with SAB final output product.

(b) The relative azimuth used by ERB is the complement of the relative azimuth as used by MLE.

(c) Underlying scene is the climatology scene used by ERBE system on the 2.5° X 2.5° grid instead of the target area system used by Nimbus-7.

(d) The bidirectional models for reflectance and the emission models are the ERBE models.

(e) Data handling and rejection of non-valid observations are different and dealt with at different locations in the code in the ERBE system. Some modifications were made to the original Langley/ NASA supplied code to handle these appropriately.

(iv) Several test runs on the data revealed a few computer-systems related problems. These were identified and corrected.

(v) Observations were truncated at different satellite zenith angles from 90° to 40° and the effect on the daily averaged instantaneous albedo, LW (day, night and total) fluxes was investigated.

Steps (vi) and (vii) were performed, using the emission models and bidirectional reflectance (ERBE) models from Nimbus-7 and directional models developed by ERBE working groups (ERBE unpublished document, 'Angular Radiation Models for ERBE': October 30, 1984).

(vi) Process each of 23 days in June 1979 through the algorithms and produce the following data sets:

(a) Average instantaneous albedo and LW flux (day, night, total) for each of the 2070 target areas on the globe.

(b) Different levels of cloudiness percentages also for each TA.

(c) All the individual converted flux and albedo values for chosen (20) TAs.

(d) All information regarding viewing and incident angles and scene selected, SW and LW radiances and the computed fluxes for 20 TAs.

(e) Statistical parameters which would provide information on the model confidence levels for all 12 surfaces.

(vii) From (vi) above, monthly averages of the parameters in (a) and (b) under (vi) for each of the TAs were computed.

(viii) SAB: From Level I data set of the SAB method, Level II algorithms were applied to create the TA averages of the instantaneous albedo and the LW fluxes. From the TA averages, the zonal and global mean values were computed. No Level III algorithms were used in the present study.

(ix) The TA zonal and global means of the parameters from SAB, and from the use of Nimbus-7 models were compared.

(x) Cloudiness percentages were converted from TA to zonal averages for each cloudiness condition from clear to completely cloudly

for each day. The percentages were plotted.

(xi) Monthly mean cloudiness percentages were computed in both cases from the daily means. Zonally averaged plots of the monthly mean cloudinesses are produced.

(xii) Similar plots were also produced for each of the studies with truncation of observations at different satellite zenith angles.

4. Results:

(Results of the validation study were presented at the ERBE Team Meeting at NASA/Langley Research Center on November 1, 1984.)

In this section, we discuss several of the results which may be classified broadly as:

(i) the final monthly mean ERB parameters

(ii) the monthly mean cloudiness - dependence on latitude band

(iii) the effect of eliminating all radiance observations beyond a satellite zenith angle

(iv) Scene Identification Reliability Index.

Several of these items have come up as offshoots of the original purpose of the study. Some of the available data and results pertaining to the 20 TAs mentioned in Section 3 (vi) C and

3 (vi) d have not been analyzed due to limited funding under the present contract.

(i) Monthly Mean Earth Radiation Budget Parameters:

These parameters are different from the conventional parameters used in most radiation budget calculations. For example, the albedo, computed and presented here is the instantaneous albedo corrected only for anisotropy of the reflecting surface and a diurnal correction is not applied. The LW fluxes are corrected for the limb brightening or darkening as the case may be. The LW flux is assumed to be constant through the night or the day, and no models are applied for the time-dependent variations. The monthly means are obtained from the daily means as simple average over the number of days used in processing. In the present case, data for 1979 are used and there are 23 days of observed data from the Nimbus-7 ERB instrument. The computed monthly mean values are shown in Table 1 as global averages. Net radiation is not obtained because the albedo presented here is not the daily mean albedo. For purposes of comparison with the validation data set, similar values obtained with SAB are also shown.

We notice from Table 1 that the global mean radiation budget parameters of interest to us, computed with the MLE method show good agreement with those obtained through the binning procedure using SAB method. Keeping all observations upto 90° in satellite zenith, the instantaneous albedo is 28.1 with the MLE method while the SAB value is 27.4. Using the bispectral threshold method applied in Nimbus-7 data processing, the monthly mean

diurnally corrected global albedo is 33.0 with a corresponding value of 30.1 from SAB method (Arking et al., 1984). Of the three ERB parameters, albedo is the one which showed worst agreement between SAB and MATRIX NFOV product. This difference of nearly 2.9 in albedo is now reduced to 0.7 with the MLE method. The improvement gets better when observations are truncated at 75° in satellite zenith angle. The LW fluxes (day time, night time and total) also improved with this truncation. The day time longwave flux difference with SAB is 2.7 w/m^2 with the SAB value at 243.7 w/m^2 and MLE value of 241.0 w/m^2. Night time and total flux values show even better agreement with SAB values. The effect of truncation at smaller angles is not appropriate and the reason will be discussed in a later section.

Differences in the zonal averages using the SAB and MLE with cutoff at 90° are shown in Fig. 3a for the albedo, and Figs. 4a, 5a, and 6a for the day time LW flux, night-time and total LW fluxes for the monthly averages respectively. On a zonal basis, the instantaneous albedoes with MLE are slightly larger by an amount smaller than 0.015 and for some latitudes in very good agreement with the SAB zonal averages. The day time LW fluxes from SAB are about 4 to 6 w/m^2 larger on an average, while the night-time values are different by about 2 watts in the same direction. The zonally averaged total LW flux is also larger (Fig. 6a) by about 3 w/m^2.

The TA fluxes with MLE are compared with those using SAB in Figures 3b, 4b, 5b and 6b. The SAB values are shown on the abscissa and the MLE values on the ordinate. The statistical parameters related to the linear regression are shown in Table 2.

Concentrating for a moment on the instantaneous albedoes, we notice that in the large albedo region, there is a good agreement between the SAB and MLE albedoes. In the low albedo region (i.e., between 0.1 and 0.3), MLE tends to overestimate the albedo by as much as 0.1 in some cases. In the intermediate albedo range, the opposite may be the case, with inaccuracies of the order of 0.05 or less.

We could conclude that in the completely cloudy and clear snow cases (high albedo), the angular models appear to behave very well while in situations of partial cloudiness as also in some clear cases, the errors vary between 0.05 and 0.1. These conclusions, however, need to be confirmed with individual albedo computations for some chosen TAs, before a final definitive conclusion can be drawn. This comparison is in progress.

On an overall basis, the albedoes with MLE are regressed against the SAB albedoes and the gradient, intercept and the coefficient of regression assuming a linear relationship are shown on the figure. The standard error of regression is 0.015. Value of σ_e, where σ_e^2 is the sum of the squares of the deviations between MLE and SAB values, is also shown on the figure.

Day time fluxes are shown in Figure 4b. The parameters of regression are also shown. The agreement at large fluxes is much better between the two methods, corresponding to warmer or non-cloudly land or desert areas. The standard error from the linear regression is about 4.5 w/m^2.

In the night time, similar results apply (Fig. 5b) except that the agreement is better in very low LW flux region. These

apparently correspond to observations from TAs which have night time all the 24 hours (or from the south polar regions and the low fluxes confirm that). From Figures 4b and 5b, we may observe that the polar long wave models are performing quite well. On a global basis, the night time LW fluxes show a smaller coefficient of regression compared to the day time or total fluxes. Similar comparisons for the total flux are shown in Fig. 6b.

Effect of eliminating observations greater than 75° is shown in Figures 7a, 8a, 9a and 10a. The zonal averages are shown as the difference between the value with SAB and the albedo with MLE when they are truncated at 75°. The regression plots are shown in the corresponding Figures 7b, 8b, 9b and 10b. The effect of truncating observations at 75° is to decrease the zonal averages of albedo generally over the southern hemisphere, and the effect is much smaller over the northern hemisphere. The LW fluxes seem to be enhanced when the observations at large satellite zenith angles (>75°) are removed and this is true in all the LW flux computations (day, night and total). In all cases, the SAB, Nimbus-75 differences are smaller than with the Nimbus-90 case.

Mercator projections of the albedo and LW flux fields between 70° S and 70°N are shown in the next 12 figures (i.e., Fig. 11 through Fig. 22. Fig. 11 through 14 are the parameter fields with the SAB method. As the earlier results showed better agreement between SAB and MLE with cutoff of 75°, the MLE results with 75° cutoff case are shown in Figs. 15 - 18. The difference plots are shown in Figs. 19-22.

(ii) Monthly Mean Cloud Percentages:

The presence or absence of a cloud and in case, a cloud is present, the degree of cloudiness is determined by the scene algorithm using the MLE probability density function. The percent cloud under each category of cloudiness is determined from the total number of observations of the TA and the number of cloud identifications in each category. The TA cloudiness categories are then composited to obtain the zonally averaged cloudiness percentages under each category for each day and the zonal monthly mean cloudinesses are computed.

Figure 23 shows the monthly mean zonal average cloudiness on the basis of the MLE method. The scene detection algorithm uses LW radiances only in the south polar regions due to the non-availability of SW radiances. All the SW and LW radiance combinations at the North Pole indicate a high degree of cloudiness near 100%. The position of the inter-tropical convergence zone seems to be very well defined slightly north of the equator and a region of high cloudiness at the South Pole. In addition, a regional peak of cloudiness in the southern hemisphere mid-latitude and a small peak and a plateau of cloudiness in the northern hemisphere mid-latitude can be observed. These may be typical of the convergence zones of the ascending portion of the Hadley cell.

Figure 24 shows the percentage clear for each latitude band in a similar way. In contrast with the cloudiness figure, not even one latitude band of the globe is completely clear. A maximum of near 55% of the zone classified as clear appears

around 40°N in June, with two peaks almost of equal percent clear in the equatorial north and south (around 20° N and 20° S respectively). The region of ITCZ clearly marked in Fig. 23 is almost 0% clear from Fig. 24 indicating that the remaining 50% of the latitude band is either partly or mostly cloudy.

Figures 25 and 26 are for the partly cloudy and mostly cloudy scene identifications and thus, complete the monthly mean picture. The winter hemisphere has greater degree of cloudiness in both these figures and in no case, do they exceed 40% of the latitude band. Combining Figures 23, 25 and 26, we would note that the degree of cloudiness is much larger in the winter hemisphere. Such a conclusion can also be drawn from looking at clear percent plot of the southern vs northern hemisphere in Figure 24.

(iii) Effect of Satellite Zenith Angle Cutoff:

(a) Budget Parameters:

Many studies analyzing the data from satellites have noted the ambiguity of scene selection at large satellite zenith (Raschke et al., 1973; Vemury et al., 1984). The effect of truncating observations at different satellite zenith angles on the albedo and LW flux have thus been investigated as a function of the satellite zenith angle. Table 3 provides a summary of the global mean values (with standard deviations) of the present set of budget parameters. They are also shown in Figures 27 and 28. The effect was studied for a day (day 152 of 1979) which happens to be the second day of a three day on and one day off cycle and thus has the maximum number of observations. As expected from earlier studies, the global albedo drops as the satellite zenith

threshold is decreased. Also, to be noted is the difference in the albedo gradient for angles 90° to 70° and for 60° to 40°. Between 70° and 60°, there is a sudden drop in the albedo. This is the region, where the number of observations by the scanner double at 58°, discussed in Vemury et al. (1984).

It is also important to note that the effect of truncation of observations also has the effect of eliminating some TAs in contributing to the global mean. In the case of instantaneous albedo, for example, during one day 1849 TAs contributed to the global mean. With a total of 2070 equal area regions, nearly 90% of the TAs participated in providing the global mean albedo. The TA sampling drops rather drastically at 40° cutoff, with only 60% of the globe by area contributing to the global mean. The situation becomes more severe for night time LW flux, where at 40 cutoff, 50% of the TAs provide a contribution to the global mean computation. In view of this reduced sampling with decreasing threshold value, it is necessary to choose a reasonable mean, where there is a compromise between the effect of incorrect scene selection and a poor sampling strategy of the global areas. The table also provides values of the LW fluxes and corresponding sample sizes for the different thresholds. As is apparent, lower than 70°, the number of TAs providing the global mean drops drastically due to the larger gradient. Thus removing too many observations (or choosing a zenith angle threshold smaller than 70°) is not a good sampling strategy.

For comparison, the values with the Nimbus-7 ERB thresholding method are shown as dashed line in Fig. 27. The scale is on the left on the inside. These are the mean daily albedo values

(Vemury et al., 1984) with bispectral thresholds, with cutoff at different angles, for June 22, 1979. It is apparent that the thresholding method for scene selection leads to a much larger decrease in albedo at almost all cutoff angles. While a perfect scene selection and correct angular models should not show any slope with satellite zenith, the result with MLE indicates that there is considerable improvement over the bispectral thresholding method.

(v) Scene Identification Reliability Index:

A measure of performance of MLE as a scene selection scheme may be obtained by defining a parameter called the Scene Identification Reliability Index. Once a scene type is chosen based on the short wave and long wave radiance measurements, this parameter indicates to within how many standard deviations, the measured and model radiance values agree. The necessary definitions are shown in Frame 6. If both SW and LW radiances are available, scene selection makes use of both these. If only the LW or the SW is available, a scene is still selected. The percentage of observations which are within one standard deviation and two standard deviations under each of the categories are shown in Table 4. Nimbus-7 bidirectional and ERBE directional models (ERBE unpublished document, 'Angular Distribution Models for ERBE', October 30, 1984) are used in this case and the results are shown for day 152 and day 153 in 1979. These percentages provide information on the level of performance of the models. For example, during the day-time for clear (0 to 5% cloud) ocean, there are 20,651 LW observations, of which 95.3% (under

NCLDAY in Table 4) are within two standard deviations of the model mean value. Of the 14,645 SW observations on the same day, almost all (99.99%) are within two standard deviations (NCSDAY in Table 4). But only 94.6% of the observations with both LW and SW measurements, are within two standard deviations for both the SW and LW. During the night time, LW only data are used and for ocean, 98.1% of the observations are within two standard deviations.

Behavior of clear snow seems to be opposite to that for ocean. During the day, 76.9% of the SW observations are within two standard deviations while nearly 96.9% of the day-time LW observations are within two standard deviations. Almost, all models seem to perform well at night. When both SW and LW observations are used, snow models behave rather poorly during the day-time with only 38.5% of the observations (SW and LW together) within two standard deviations. Day-time desert observations seem to be in quite good agreement with model expectations for the SW (98.0% within two standard deviations), while for the long wave, the percentage drops to 68.7%.

These different results for the 12 identified surfaces are shown in Fig. 29 for the case of the index less than or equal to 2. For all the mostly cloudy scenes and for the overcast case, the observations seem to be in very good agreement with the models at the 2σ level, while the snow model seems to be the worst, followed by the desert model. Similar histogram of the model performance index at the 1σ level is presented in Fig. 30.

The "overall model" performance for the day is obtained from the bottom line of Table 4 for day 152. When both SW and LW

radiances are used, 90.3% of the 163,670 observations are within 2σ of the respective chosen models. During the night time, 96.13% of the 229,946 observations are within 2σ .

The model reliability parameters thus indicate that the scene identification method is picking the scenes consistent with the angular model statistics. The better performance at night is not necessarily due to the models being more appropriate for night, but that the bidirectional model standard deviations for LW are much smaller than the SW standard deviations.

5. Conclusions

1. Maximum Likelihood Estimation method provides albedoes and LW fluxes in very good agreement with the SAB method.

2. MLE method has improved the scene selection compared to the bispectral threshold method. The albedo decrease (due to incorrect scene) is considerably reduced (Fig. 27).

3. Adequate sampling strategy requires that satellite zenith angle cutoff should not be lower than 70°.

4. There is still a remnant of the scene id. problem. Part of this may be due to the angular models as well.

5. As a test of the software, the scene id. algorithm is performing well and there are no surprises.

6. MLE procedure could pick out all scenes including partly cloud scenes.

6. Future ERBE-Related Studies

A. Comparison of ERB parameters on a regional or target area basis between SAB and MLE methods.

B. Effect of GOES models (monthly).

C. Effect of zenith angle cutoff with GOES models.

D. Sensitivity of scene selection to LW-SW correlation coefficients.

E. Are LW models adequate?

F. Conduct experiments to determine the uncertainty in the flux measurements.

G. Validate scene selection from other data sets.

H. Continue similar studies for at least one more month.

7. Acknowledgements:

We gratefully acknowledge the encouragement and support from several members of the ERBE team, in particular B. Wielecki and J. T. Suttles. M. King of NASA/GSFC has provided useful occasional criticisms and kindly made the computer resources available on the SACC computer. Acknowledgements are also due to H. Lee Kyle of NASA/GSFC for providing the necessary datasets and some portions of the Nimbus-7 ERB software and to Ravi Govindaraju, who has painstakingly developed and modified several sections of the software, for his programming support. M. Dean has kindly typed several versions of this report.

8. References

Arking, A., and S. Vemury, "The NIMBUS-7 ERB Data Set: A Critical Analysis", J. Geophys. Res., Vol. 89, NO. D4, 5089-5097, 1984.

Chen, T.S., L.L. Stowe, V.R. Taylor, and F.P. Clapp, Classification of Clouds using THIR Data From Nimbus-7 Satellites, paper presented at Proceedings of International Radiation Symposium, Ft. Collins, Co., 1980.

Hwang, P.H. (Ed) Nimbus 7 THIR Users' Guide, NASA Goddard Space Flight Center, Greenbelt, MD., 1982.

Jacobowitz, H., H.V. Soule, H. Lee Kyle, F.B. House, and the Nimbus-7 ERB Experiment Team, "The Earth Radiation Budget (ERB): An Overview", J.G.R., Vol. 89, No. D4, pp 5021-5038, 1984.

Raschke, E., T.H. Vonder Haar, W.R. Bandeen, and M. Pasternak, "The Annual Radiation Balance of the Earth-Atmosphere System During 1969-70 From Nimbus-3 Measurements", J. Atmos. Sci., 30, 341-364, 1973.

Ruff, I., R. Koffler, S. Fritz, J.S. Winston and P.K. Rao, "Angular Distribution of Solar Radiation Reflected From Cloud as Determined From TIROS-IV Radiometer Measurements", J. Atmos. Sci., 25, 323-332, 1968.

Vemury, S.K., L. Stowe, H. Jacobowitz, "Sample Size and Scene Identification (Cloud): Effect on Albedo", J.G.R., Vol. 89, No. D4, pp 5345-5353, 1984.

9.

Frames

Definitions

S' : Instantaneous solar irradiance measurement

$= S_o (d/d_o)^2$

ζ' : Solar zenith angle at the time of measurement

$N_f(\zeta')$: Filtered radiance (measurement)

$N_{R,E}(\zeta')$: Unfiltered radiance (after spectral correction)
R= Reflected; E= Emitted

θ : Satellite zenith angle

ϕ : Relative azimuth

Frame 1

Bidirectional Reflectance:

$$\rho(\zeta') = \frac{N(\zeta')}{S' \cos\zeta'} \tag{1}$$

Directional Reflectance:

$$r(\zeta') = \int_0^{2\pi} \int_0^1 \rho(\zeta') \sin\theta \, d(\sin\theta) \, d\phi \tag{2}$$

Normalized Reflectance:

$$\frac{r(\zeta)}{r(\zeta=0)} = R(\zeta) \tag{3}$$

Instantaneous Albedo

$$= \frac{\pi N_R(\zeta')}{S' \cos\zeta'} \tag{4}$$

Angular Model Correction Factor:

$$A(\bar{\zeta}';\theta,\phi) = \frac{\pi \bar{N}_R(\bar{\zeta}',\theta,\phi)}{\int_0^{2\pi} \int_0^{\pi/2} \bar{N}_R(\bar{\zeta}',\theta,\phi) \sin\theta \, d(\sin\theta) \, d\phi} \tag{5}$$

Instantaneous Corrected Albedo:

$$\frac{\pi N_R(\zeta')}{S' \cos\zeta'} \Big/ A(\zeta';\theta,\phi) \tag{6}$$

Bidirectional Reflectance

$$\rho_{j,k,n} = \frac{\pi N'_{j,k,n}}{S_o (d/d_o)^2 \cos \zeta'} \qquad (7)$$

where $j = 1,.....m$ (observation number)

$k = 1,.....85$ (Bin # in TA n)

$n = 1,.....2070$ (TARGET AREA #)

f_j = Fractional Field of View belonging to the TA n.

Instantaneous Corrected Albedo for bin k

$$A_{k,n} = \sum_{j=1}^{m} f_j \rho_{j,k,n} f_{A,\zeta'} \Big/ \sum_{j=1}^{m} f_j \qquad (8)$$

(In this case $f_{A,\zeta'}$ is set equal to 1)

$$\omega_k = \Delta\Omega_k = \cos\theta \sin\theta \, d\theta \, d\phi)_{\text{kth bin}}$$

$$\text{Instantaneous Target Area Albedo} = \sum_{k=1}^{85} A_{k,n} \omega_k \qquad (9)$$

SAB

1. STR tapes are used due to data compaction.

2. Data quality is high due to severe quality control checks.

3. Solar zenith angle information on the STR tapes is not precise.

4. Fields of view which belong to different TAs are apportioned by the proper fraction of the radiance to each TA.

5. Target Areas are rejected if

   a) the total sample size is less than 300.

   b) the center bin has less than 5 observations.

   c) any TA with more than 8 bins that have less than 5 observations.

6. If a Target Area is accepted, any empty bins are filled by interpolation from the near neighbors.

7. The radiance means are computed and weighted by the solid angle of the bin and integrated over the 85 bins to obtain the TA flux.

8. The zonal and global averages are calculated form the TA fluxes.

Frame 3 (Contd.)

MAXIMUM LIKELIHOOD ESTIMATION

REQUIRED SUBSIDIARY DATA SET

From NIMBUS-7 Scanner Database

I. BIDIRECTIONAL MODELS (REFLECTANCE)

- (A) For each of 10 solar zenith angle ranges
- (B) For each of 12 scene types
- (C) For each of 49 angular bins
  - (i) Obtain mean SW and LW ansotropic factors
  - (ii) Obtain standard deviations
  - (iii) Obtain correlation coefficients

II. DIRECTIONAL MODELS (REFLECTANCE)

- (A) For each of 12 scene types
- (B) For 10 solar zenith intervals
  - i) Albedo values
  - ii) Normalized (to nadir) reflectances

III. LONGWAVE MODELS (EMISSION)

- (A) For each of 10 Latitude bands
- (B) For each of 7 Satellite zenith intervals
  - i) Amisotropic correction factors for the LW radiance to flux conversion
  - ii) A priori Longwave mean values

GEOGRAPHY DATASET

A global dataset of surface classification on a $2 \cdot 5^{\circ} \times 2 \cdot 5^{\circ}$ grid into ocean, land, snow, desert and mixes land/ocean areas.

ASSUMPTIONS FOR APPLYING MLE:

(A) That each set of SW, LW radiance measurements under each of the above cases is completely independent of other observations (statistical independence of the sample)

(B) That the sample size is adequate and that the samples are distributed randomly to constitute a normal distribution

(C) Complete sample of SW, LW radiances belongs to a bivariate normal distribution.

Frame 4 (Cont'd)

COMPUTATION: Probability density function under condition -CND is

$$P\left[M^{SW}, M^{LW}\right]_{CND} =$$

$$\frac{1}{2\pi\,\sigma_{CND}(SW)\,\sigma_{CND}(LW)} \times \frac{e^{-Q_{CND}}}{\sqrt{1-\rho_{CND}^2}}$$

where

$$Q_{CND} = \frac{1}{2(1-\rho_{CND}^2)}\left[\left\{\frac{\left(M^{SW}-L_{CND}^{SW}\right)}{\sigma_{CND}(SW)}\right\}^2 + \left\{\frac{\left(M^{LW}-L_{CND}^{LW}\right)}{\sigma_{CND}(LW)}\right\}^2 - 2\,\rho_{CND}\left\{\frac{\left(M^{SW}-L_{CND}^{SW}\right)\left(M^{LW}-L_{CND}^{LW}\right)}{\sigma_{CND}(SW)\,\sigma_{CND}(LW)}\right\}\right]$$

P is probability density

CND is one of four conditions of the viewed surface, viz., clear, partly cloudy, mostly cloudy or overcast

σ is standard deviation from the model

ρ is correlation ceofficient

M Measured radiance values

L Apriori radiance values

PROCEDURE: To identify scene, compute P for each of the 4 conditions for the viewed surface; pick the scene which has the maximum probability density function P.

Frame 5

SCENE ID RELIABILITY CRITERIA

$$LW\ DISP = (N_{LW,\,MEAS} - N_{LW,\,MODEL}) \Big/ \sigma_{LW,\,MODEL}$$

$$SW\ DISP = (N_{LW,\,MEAS} - N_{SW,\,MODEL}) \Big/ \sigma_{SW,\,MODEL}$$

$NCLA \leqslant 2 \Longrightarrow LW.DISP \leqslant 2$ AND $SW.DISP \leqslant 2$

$NCLDAY \leqslant 2 \Longrightarrow LW.DISP \leqslant 2$ (DAYTIME LW DATA ONLY)

$NCLNIT \leqslant 2 \Longrightarrow LW.DISP \leqslant 2$ (NIGHT LW DATA ONLY)

$NCSDAY \leqslant 2 \Longrightarrow SW.DISP \leqslant 2$ (DAYTIME SW DATA ONLY)

10. List of Tables

Table 1: Monthly mean global averages of the radiation budget parameters computed using i) SAB method ii) MLE method with Nimbus-7 models with zenith angle cutoff at 90° and 75°.

Notice that the agreement is better with SAB when Nimbus-7 models with cutoff at 75° are used.

Table 2: Regression relations for the SAB - Nimbus comparisons.

Table 3: Effect of zenith angle cutoff of observations on the instantaneous albedo, LW (Day, Night and Total) fluxes for Day 152 (June 1, 1979).

The corresponding sample sizes are shown in Table 3B.

Table 4: Scene Reliability Index for each scene and cumulative value for the entire globe for Day 152 and Day 153. Nimbus-7 models are used.

Table 1

COMPARISON OF GLOBAL AVERAGES

SAB AND MLE METHODS

MONTHLY MEANS FOR JUNE 1979

	SAB	MLE	
		SAT.ZEN $\leq 90°$ **	SAT.ZEN $\leq 75°$
Inst. Albedo	*0.2738	0.2813	0.2804
LW Flux (Day)	243.7	237.7	241.0
LW Flux (Night)	232.8	229.7	232.2
LW Flux (Total)	235.6	231.8	234.7

* With Diurnal Correction: NFOV (SAB) ALBEDO = 0.301

NFOV (MATRIX) ALBEDO = 0.330

** This case is referred to as the Nimbus-90 (N90) case through out the report to indicate that results obtained with MLE with Nimbus-7 models with all observations up to 90° in satellite zenith angle. Under similar conditions when observations are limited to 75° in the zenith angle, the results are referred to as Nimbus-75 (N75).

Table 2

		A*	B	R	σ^2
Inst. Albedo	(N75)	0.017	0.960	0.993	0.2227×10^{-3}
	(N90)	0.018	0.968	0.992	0.2402×10^{-3}
Day (LW)	(N75)	-0.032	0.995	0.998	15.67
	(N90)	0.715	0.978	0.997	19.75
Night (LW)	(N75)	-0.889	1.002	0.997	13.63
	(N90)	-1.196	0.992	0.996	20.91
Total (LW)	(N75)	-2.044	1.005	0.997	8.598
	(N90)	-1.290	0.989	0.995	12.953

* Regression parameters
A = Intercept
B = Gradient
R = Correlation Coefficient
σ^2 = Standard error

Table 3.

DSNAME=W5SKV.LIB.MLE (DLGLBTBL)

MLE

DAILY
GLOBAL AVERAGES
JUNE 1ST 1979

DESCRIPTION	NIMBUS (90 DEG)	NIMBUS (80 DEG)	NIMBUS (70 DEG)	NIMBUS (60 DEG)	NIMBUS (50 DEG)	NIMBUS (40 DEG
DAILY MEAN ALBEDO	0.2812	0.2802	0.2787	0.2727	0.2693	0.266
LONG WV.FLUX (DAY)	236.7007	239.5793	241.5121	242.1980	242.7481	243.595
LONG WV.FLUX (NIGHT)	228.1264	231.0569	232.5696	232.6121	232.6225	231.838
TOTAL	230.5099	233.3534	235.3143	235.7682	236.3256	236.467

00010003
00020007
00030007
00040007
00050007
00060007
00070007
00080007
00090007
00110007
00120007
00130007
00140007
00150007
00160007
00170007
00180007
00190007
00200007
00210007
00220007
00230007
00240007
00250007
00260007
00270007
00280007
00290007
00300007
00310007
00320007
00330007
00340007
00350007

Table 3(a).

SAMPLE SIZES

Number of TAs Used — Max. Number = 2070 TAs

DESCRIPTION	NIMBUS (90 DEG)	NIMBUS (70 DEG)	NIMBUS (60 DEG)	NIMBUS (50 DEG)	NIMBUS (40 DEG)
Inst. Albedo	1849	1828	1717	1507	1204
LW Flux (Day)	1849	1828	1717	1507	1201
LW Flux (Night)	1781	1741	1583	1345	1088
LW Flux (TOTAL)	2070	2070	2040	1919	1672

Table 4.

****
* NIMBUS-7 *
****

******** DAY 152 **********

	NCLA			NCLDAY			NCLNIT			NCSDAY		
	TOTAL	PRCNT .LE.1	PRCNT .LE.2	TOTAL	PRCNT .LE.1	PRCNT .LE.2	TOTAL	PRCNT .LE.1	PRCNT .LE.2	TOTAL	PRCNT .LE.1	PRCNT .LE.2
OCEAN	14645	0.6682	0.9460	20651	0.7146	0.9529	21278	0.8067	0.9808	14645	0.9717	0.9999
LAND	9997	0.3792	0.8436	13557	0.5354	0.8655	7665	0.8843	0.9956	9997	0.7620	0.9908
SNOW	13	0.0000	0.3846	1051	0.9163	0.9686	6110	0.6810	0.9989	13	0.1538	0.7692
DESRT	5029	0.2490	0.6542	6669	0.3734	0.6866	3631	0.7761	0.9956	5029	0.6767	0.9801
MIXED LAND/OCEAN	1349	0.5374	0.9222	1838	0.6028	0.9255	939	0.8839	0.9968	1349	0.9155	0.9948
PARTLY CLOUDY/OCEAN	15854	0.6659	0.9806	21509	0.7934	0.9858	24503	0.9836	1.0000	15854	0.9225	0.9999
PARTLY CLOUDY/LAND	6806	0.4954	0.9483	9593	0.8985	0.9756	7132	0.9933	1.0000	6806	0.5886	0.9815
PARTLY CLOUDY/LAND,OCEAN MIX	784	0.6110	0.9222	1059	0.8074	0.9424	736	0.9986	1.0000	784	0.7985	1.0000
MOSTLY CLOUDY/OCEAN	22972	0.5022	0.9595	30982	0.7069	0.9710	37653	0.8301	0.9972	22972	0.7501	0.9962
MOSTLY CLOUDY/LAND	4692	0.4454	0.9197	6443	0.8006	0.9781	8325	0.9216	0.9950	4692	0.6023	0.9425
MOSTLY CLOUDY/LAND,OCEAN MIX	739	0.5074	0.9499	1033	0.7202	0.9632	762	0.9213	1.0000	739	0.7713	0.9946
COMPLETELY CLOUDY	80790	0.4821	0.8820	107999	0.6797	0.9202	111212	0.6697	0.9255	80790	0.6686	0.9415
	163670	0.5066	0.9034	222384	0.6939	0.9310	229946	0.7731	0.9613	163670	0.7356	0.9669

******** DAY 153 **********

	NCLA			NCLDAY			NCLNIT			NCSDAY		
	TOTAL	PRCNT .LE.1	PRCNT .LE.2	TOTAL	PRCNT .LE.1	PRCNT .LE.2	TOTAL	PRCNT .LE.1	PRCNT .LE.2	TOTAL	PRCNT .LE.1	PRCNT .LE.2
OCEAN	14193	0.6815	0.9490	19627	0.7264	0.9569	19967	0.8142	0.9833	14193	0.9704	0.9994
LAND	9889	0.3536	0.8387	13210	0.5213	0.8548	8900	0.8522	0.9967	9889	0.7515	0.9913
SNOW	22	0.0909	0.8182	825	0.9321	0.9927	4956	0.5920	1.0000	22	0.3636	0.8636
DESRT	5015	0.2497	0.6949	6752	0.3826	0.7167	3528	0.8339	0.9989	5015	0.6279	0.9743
MIXED LAND/OCEAN	1258	0.5668	0.9515	1678	0.6514	0.9583	1301	0.8148	0.9992	1258	0.8824	0.9968
PARTLY CLOUDY/OCEAN	15682	0.6406	0.9798	20950	0.7633	0.9850	24049	0.9838	1.0000	15682	0.9333	0.9999
PARTLY CLOUDY/LAND	6031	0.5341	0.9572	8741	0.9119	0.9815	9039	0.9933	1.0000	6031	0.6201	0.9833
PARTLY CLOUDY/LAND,OCEAN MIX	760	0.5316	0.8921	989	0.7462	0.9171	1013	0.9990	1.0000	760	0.7474	1.0000
MOSTLY CLOUDY/OCEAN	19583	0.4863	0.9598	26979	0.7101	0.9723	38479	0.8286	0.9977	19583	0.7207	0.9944
MOSTLY CLOUDY/LAND	4461	0.4885	0.9451	6187	0.8185	0.9819	8636	0.9089	0.9954	4461	0.6499	0.9662
MOSTLY CLOUDY/LAND,OCEAN MIX	713	0.4670	0.9201	940	0.7021	0.9500	1040	0.8971	1.0000	713	0.7153	0.9860
COMPLETELY CLOUDY	74098	0.4828	0.8892	99180	0.6632	0.9231	109070	0.6912	0.9465	74098	0.6950	0.9495
	151705	0.5050	0.9086	206050	0.6840	0.9328	229978	0.7848	0.9725	151705	0.7478	0.9714

11. Figure Captions

Fig. 1: Target Area (TA) sampling using SAB method. Number of rejected TAs in each of the 40 latitude bands are shown by the dashed line. The solid line indicates the total number of TAs in the latitude band. Results are for the reflected flux.

Fig. 2: Same as Fig. 1. The results are for the case of night-time emitted flux.

Fig. 3: a) SAB, MLE 90° cutoff comparison. Differences of zonally averaged monthly mean albedo between the two methods.

b) Linear regression relation between MLE with cutoff at 90° and SAB for albedo. The derived regression line parameters along with coefficient of correlation and the standard error of estimate are shown. Also shown is the value σ_e where σ_e^2 is the sum of the squares of the deviations.

Fig. 4: a) Same as Fig. 3(a) for Day time LW flux differences.

b) Same as Fig. 3(b) for Day time fluxes.

Fig. 5: a) Same as Fig. 3(a) for Night time LW flux differences.

b) Same as Fig. 3(b) for Night time fluxes.

Fig. 6: a) Same as Fig. 3(a) for Total LW flux differences.

b) Same as Fig. 3(b) for Total fluxes.

Figs. 7-10: Same as Figs. 3-6 with the MLE method. Observations with satellite zenith angle greater than 75° are removed.

Figs. 11-14: Mercator maps of instantaneous albedo and Long wave flux fields (Day time, Night time and Total Long wave) between 70 S and 70 N. SAB method is used.

Figs. 15-18: Mercator maps of instantaneous albedo and LW flux fields between 70 S and 70 N. MLE method, with cutoff at 75 in satellite zenith and with Nimbus-7 models, is used.

Figs. 19-22: Mercator projection of ERB parameter difference fields between SAB and MLE with cutoff in satellite zenith at 75 .

Figs. 23-26: Monthly zonally averaged clear and cloudy scene percentages with the use of Nimbus-7 models. Completely cloudy - Fig. 23; Clear - Fig. 24; Partly cloudy - Fig. 25; Mostly cloudy - Fig. 26.

Fig. 27: Instantaneous albedo with different zenith thresholds for Day 152. Results with bispectral thresholds are shown for comparison.

Fig. 28: LW fluxes for Day 152 as a function of zenith angle cutoff.

Figs. 29-30: Scene Id. Reliability Index for the 12 scenes at the 2σ and 1σ levels for June 1, 1979. The terms NCLA etc. are defined in Frame 6.

JUNE 1979; REJECTED VERSUS TOTAL TARGET AREAS; REFLECTED;

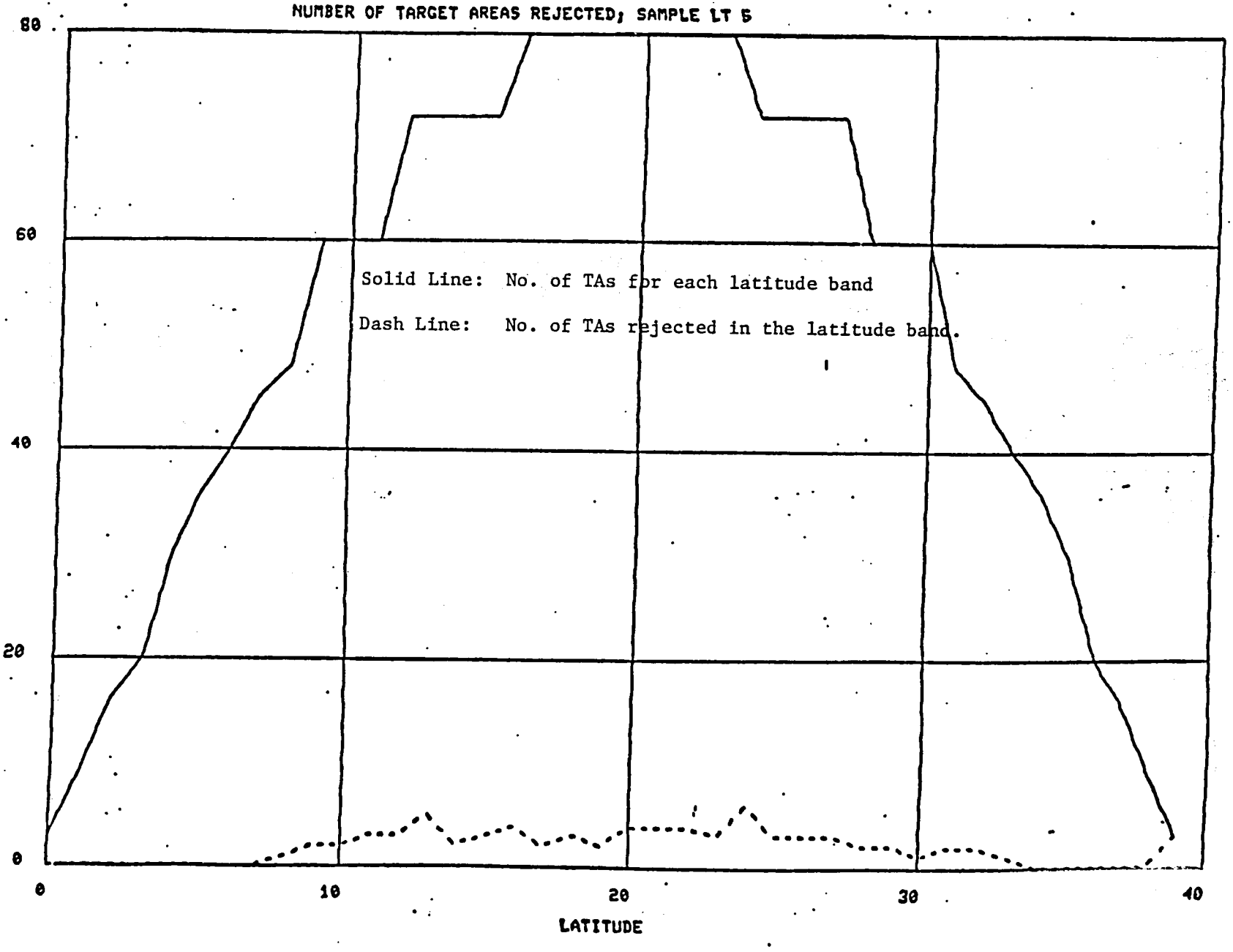

Figure 1.

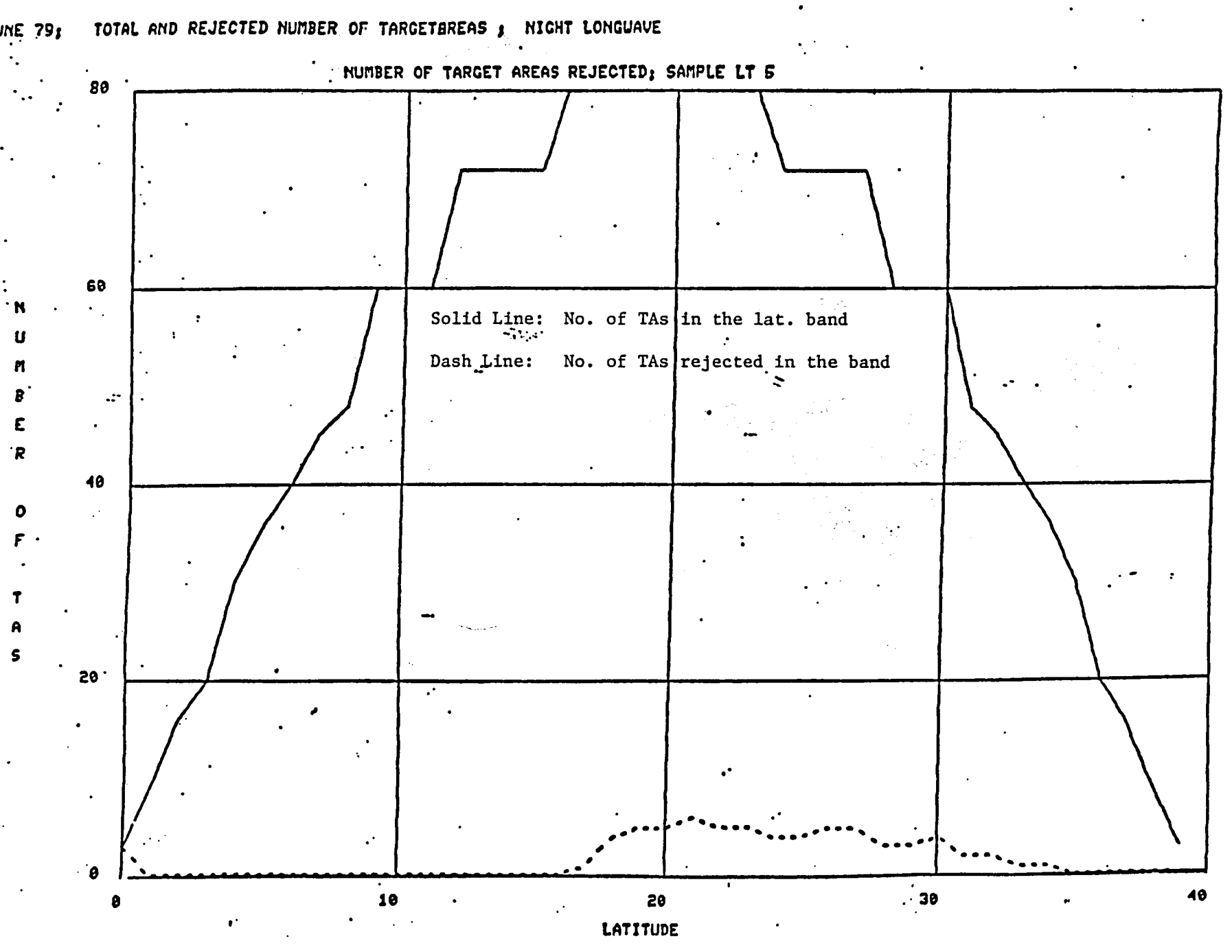
JUNE 79; TOTAL AND REJECTED NUMBER OF TARGETAREAS ; NIGHT LONGWAVE
NUMBER OF TARGET AREAS REJECTED; SAMPLE LT 5
Solid Line: No. of TAs in the lat. band
Dash Line: No. of TAs rejected in the band
NUMBER OF TAS
LATITUDE
0
20
40
60
80
0
10
20
30
40

Figure 2.

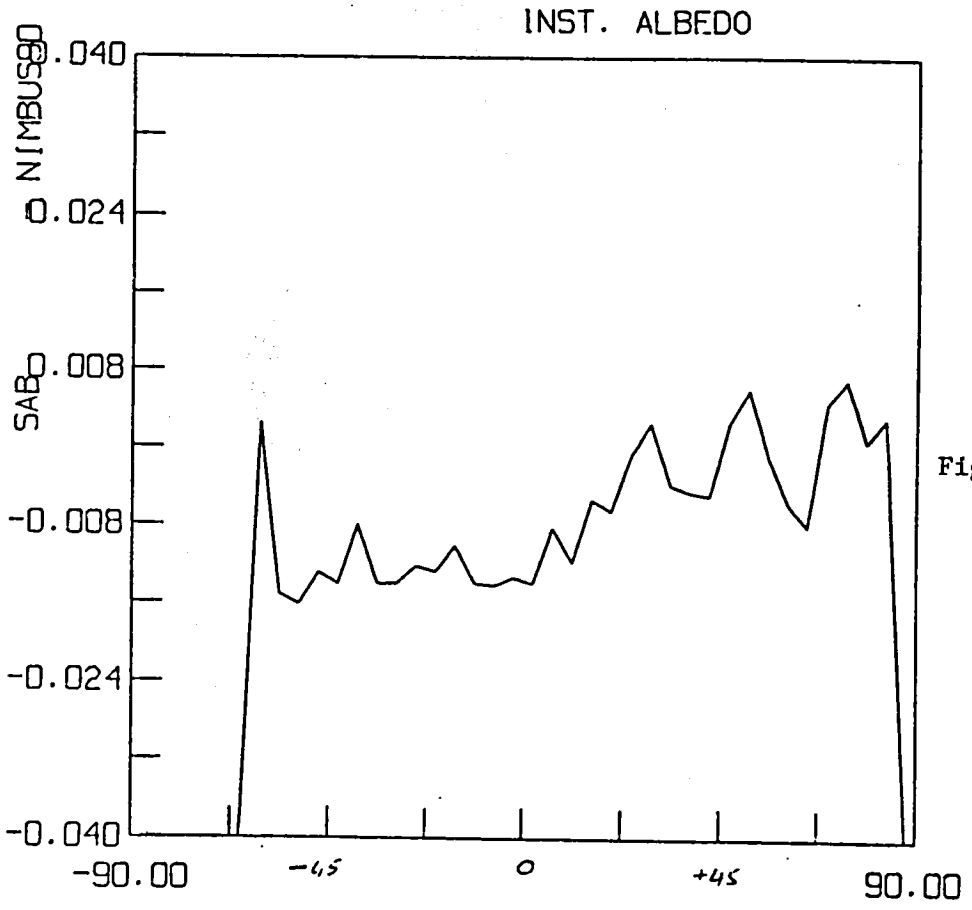

Figure 3a

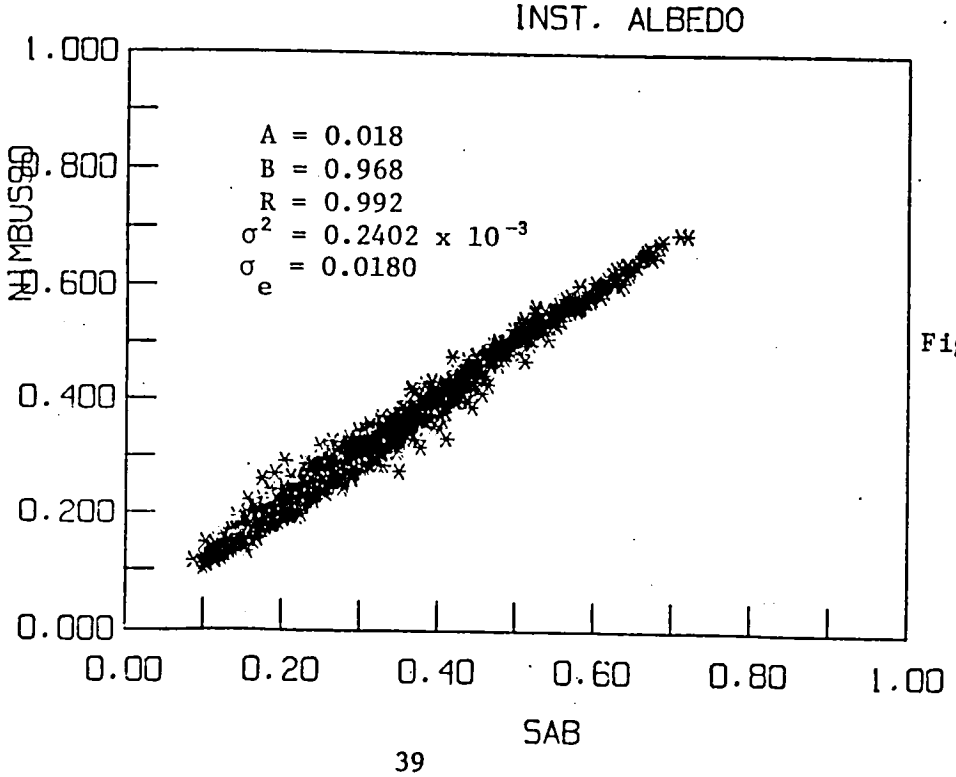

Figure 3b

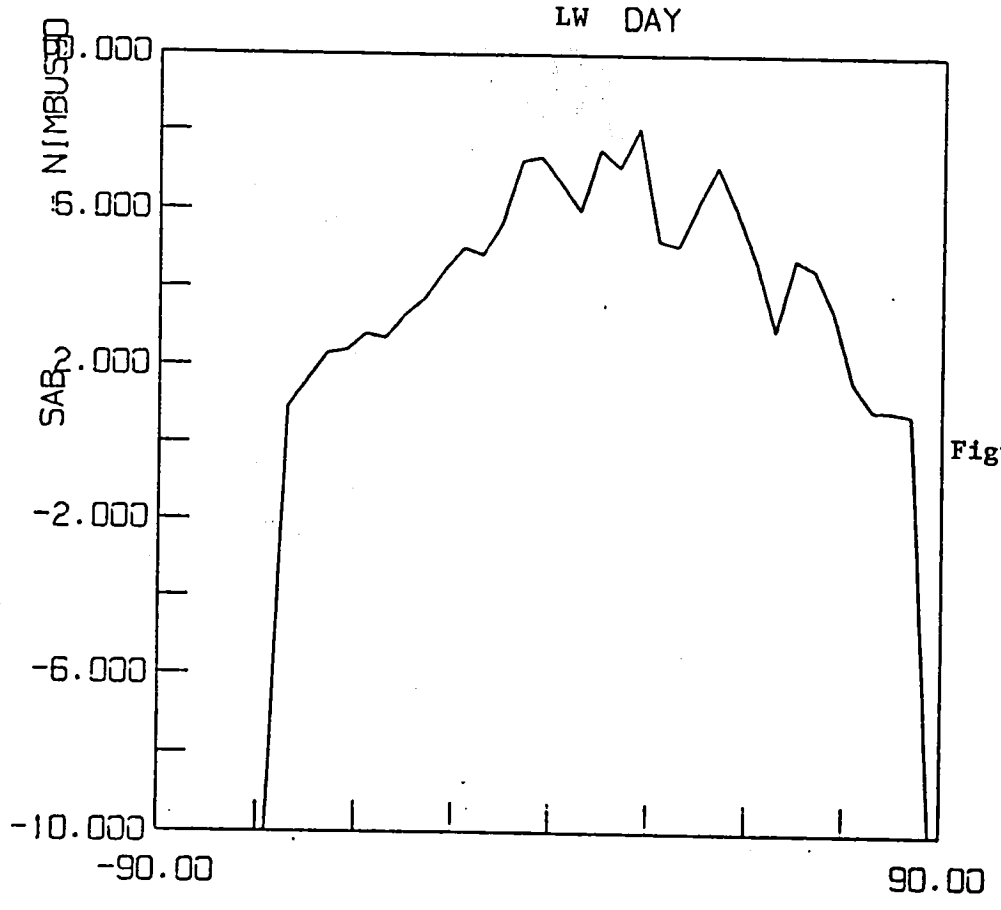

Figure 4a

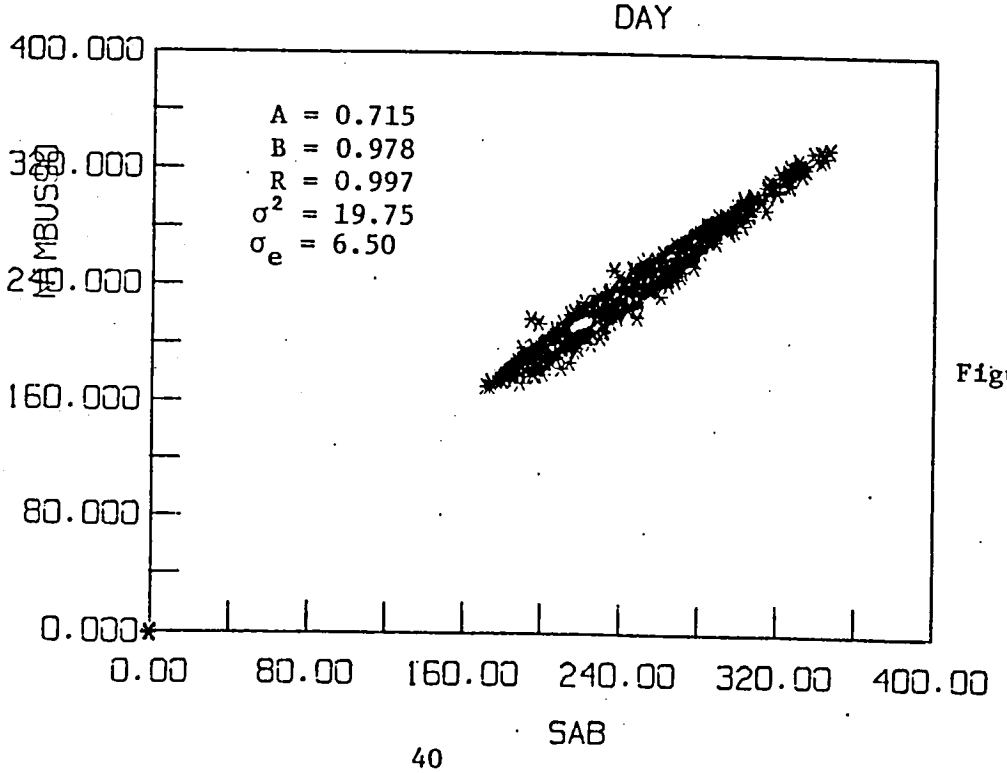

Figure 4b

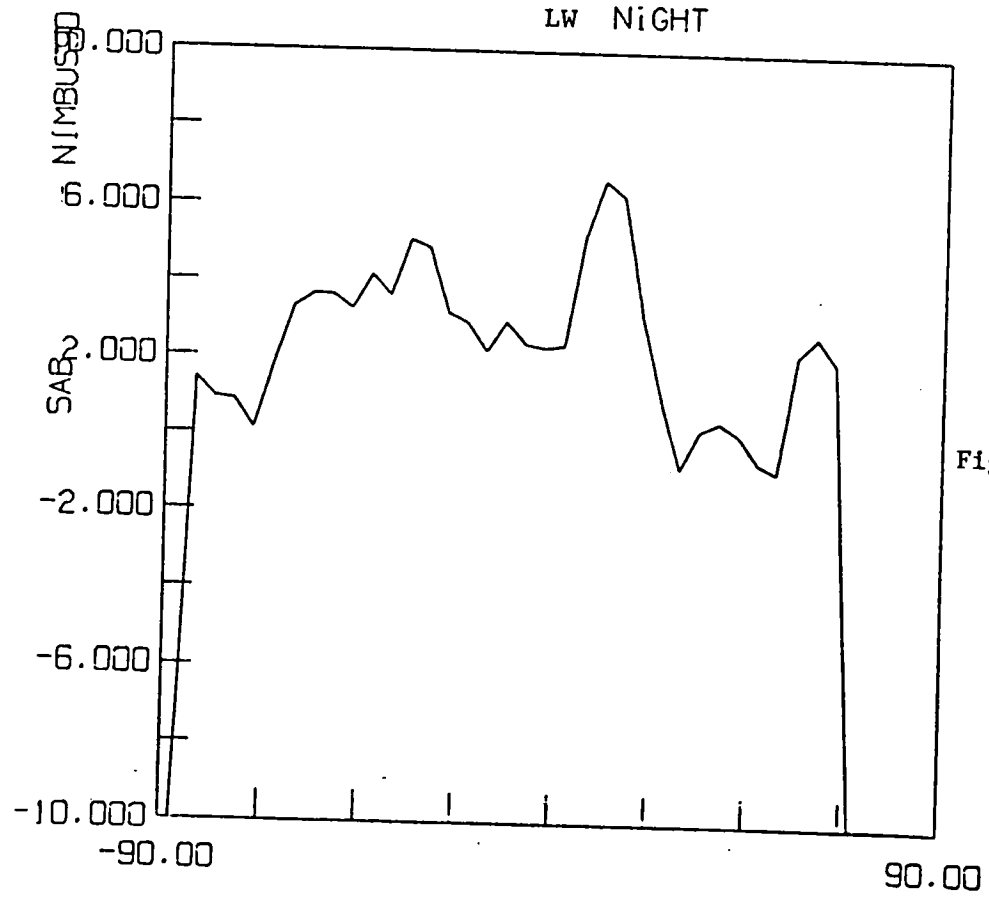

Figure 5a

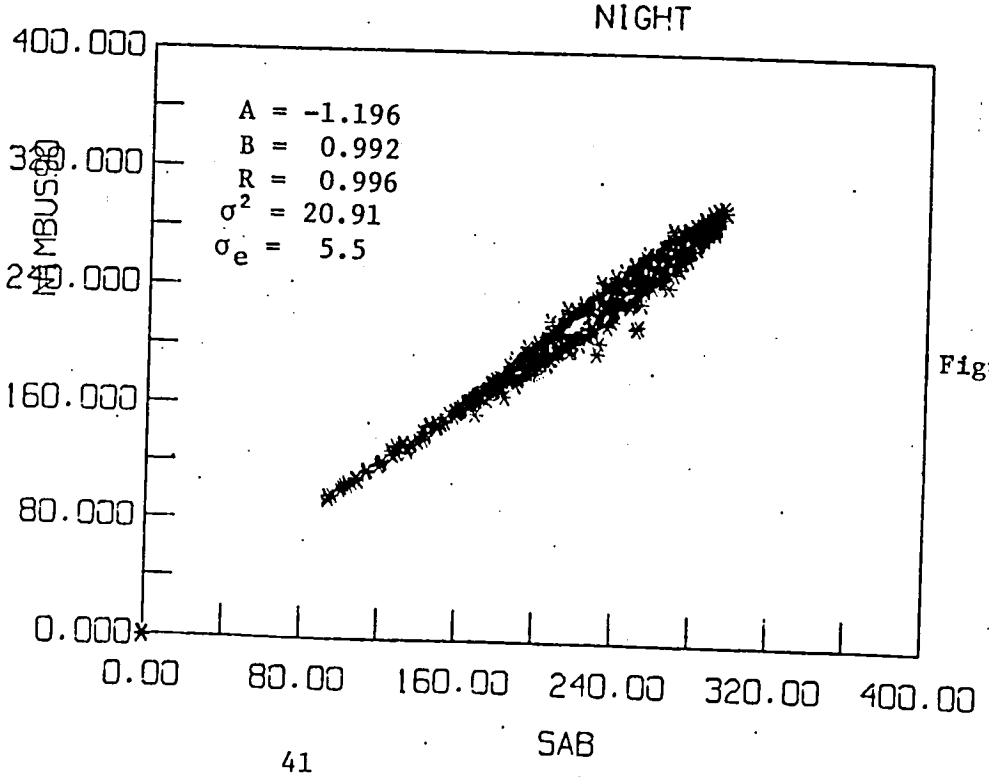

Figure 5b

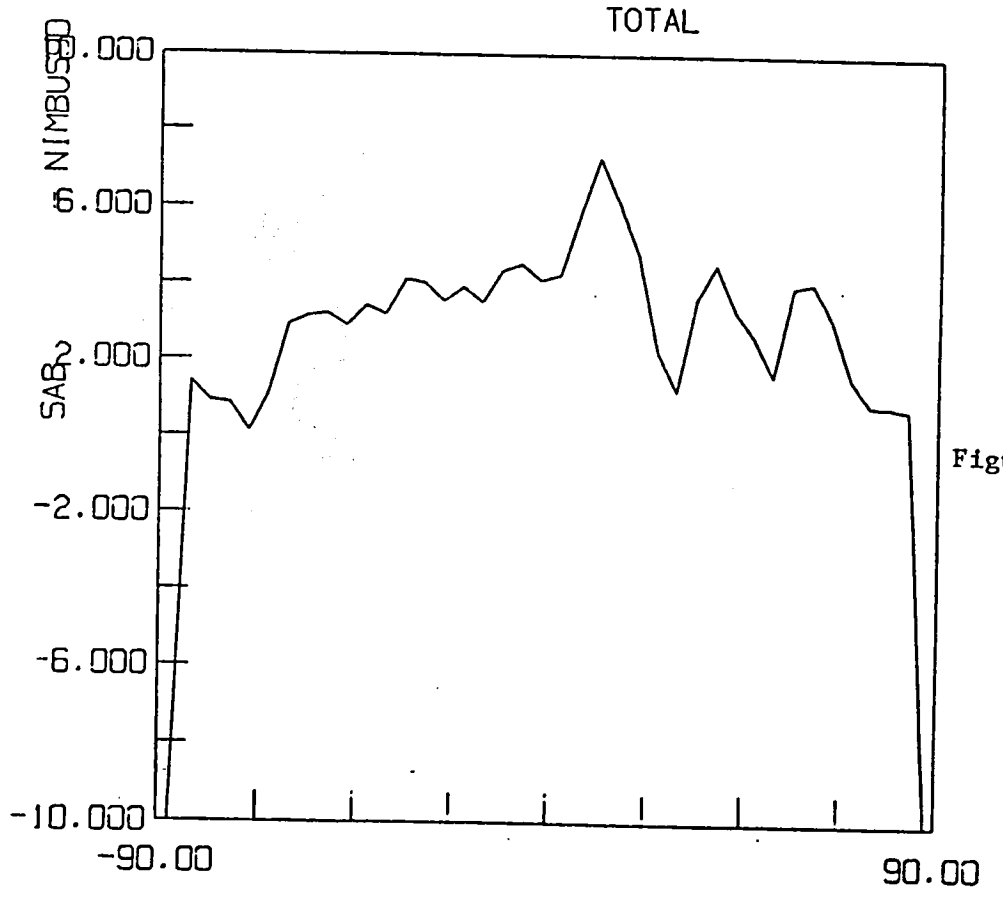

Figure 6a

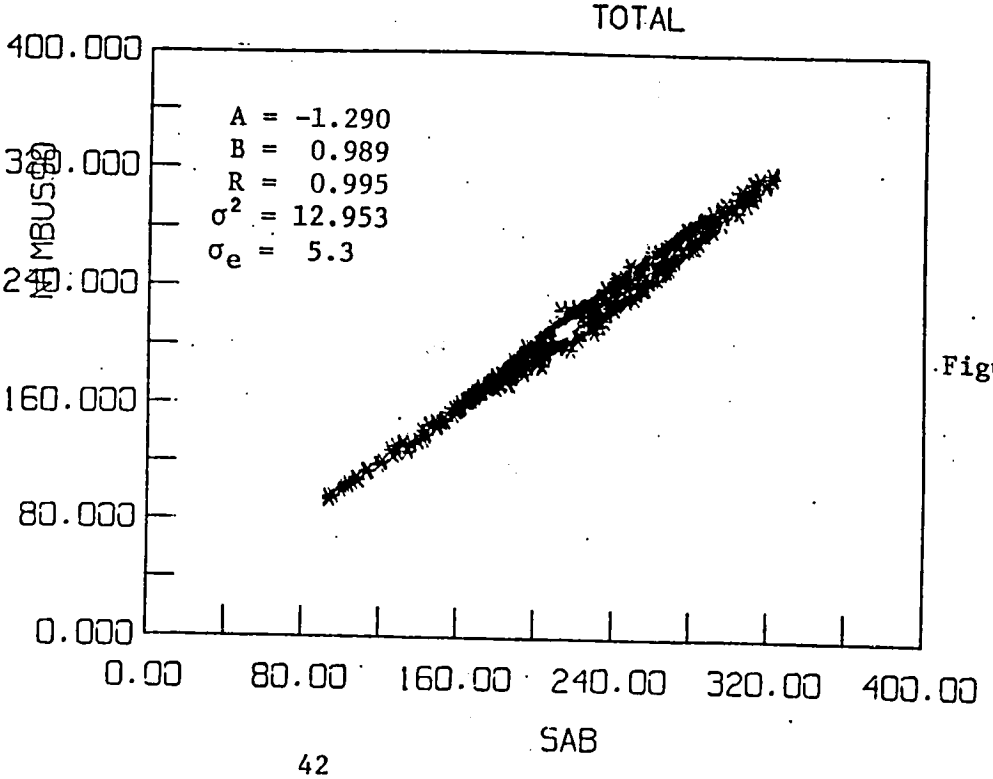

Figure 6b

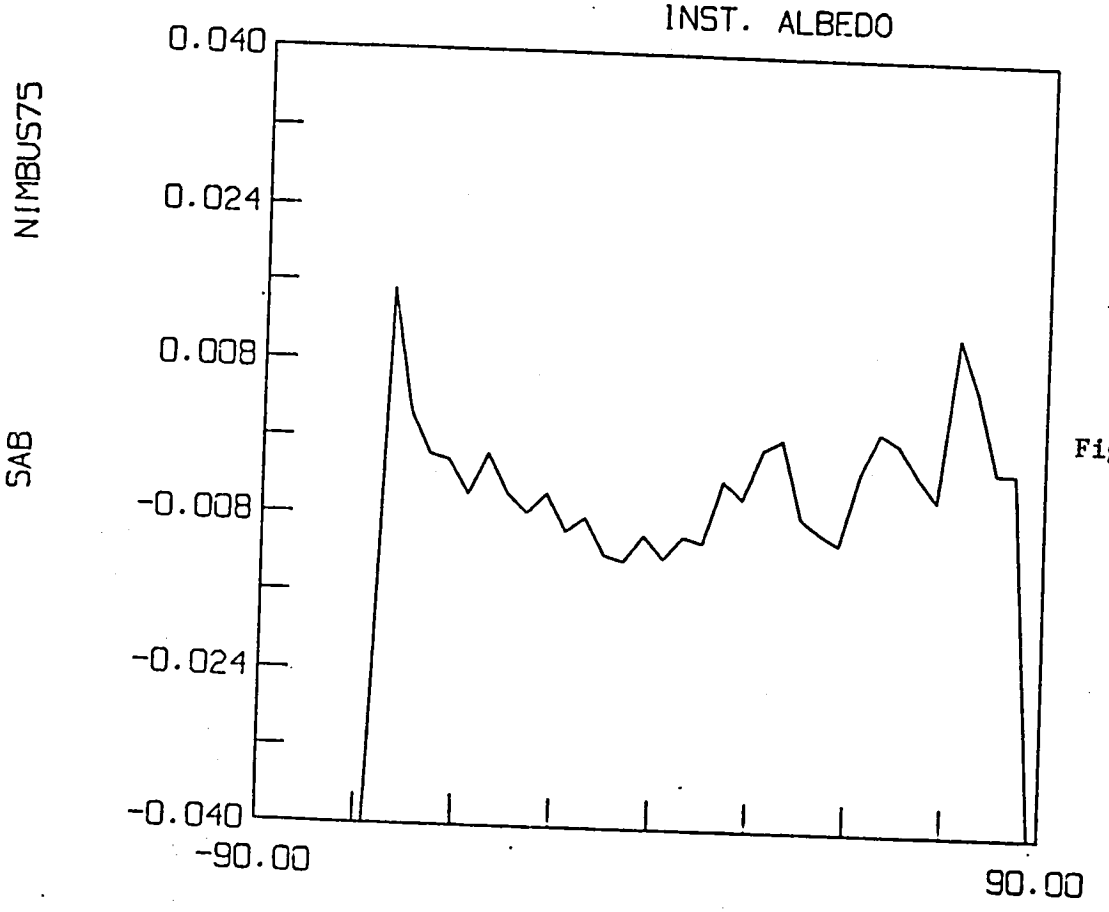

Figure 7a

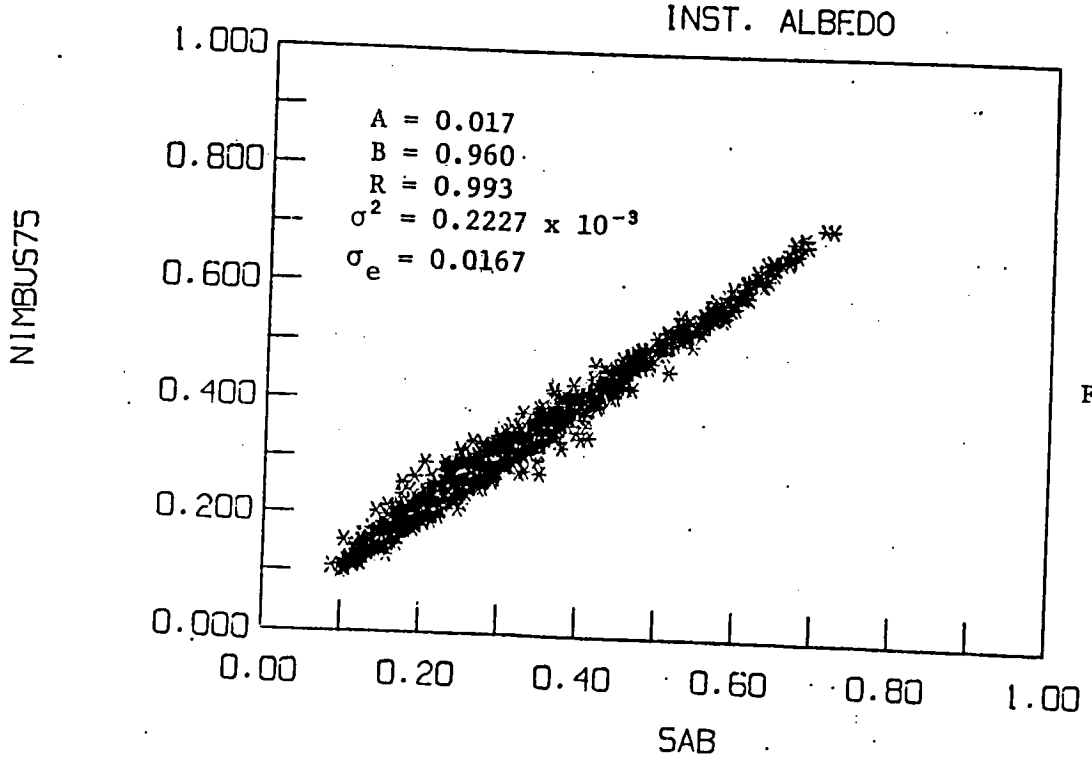

Figure 7b

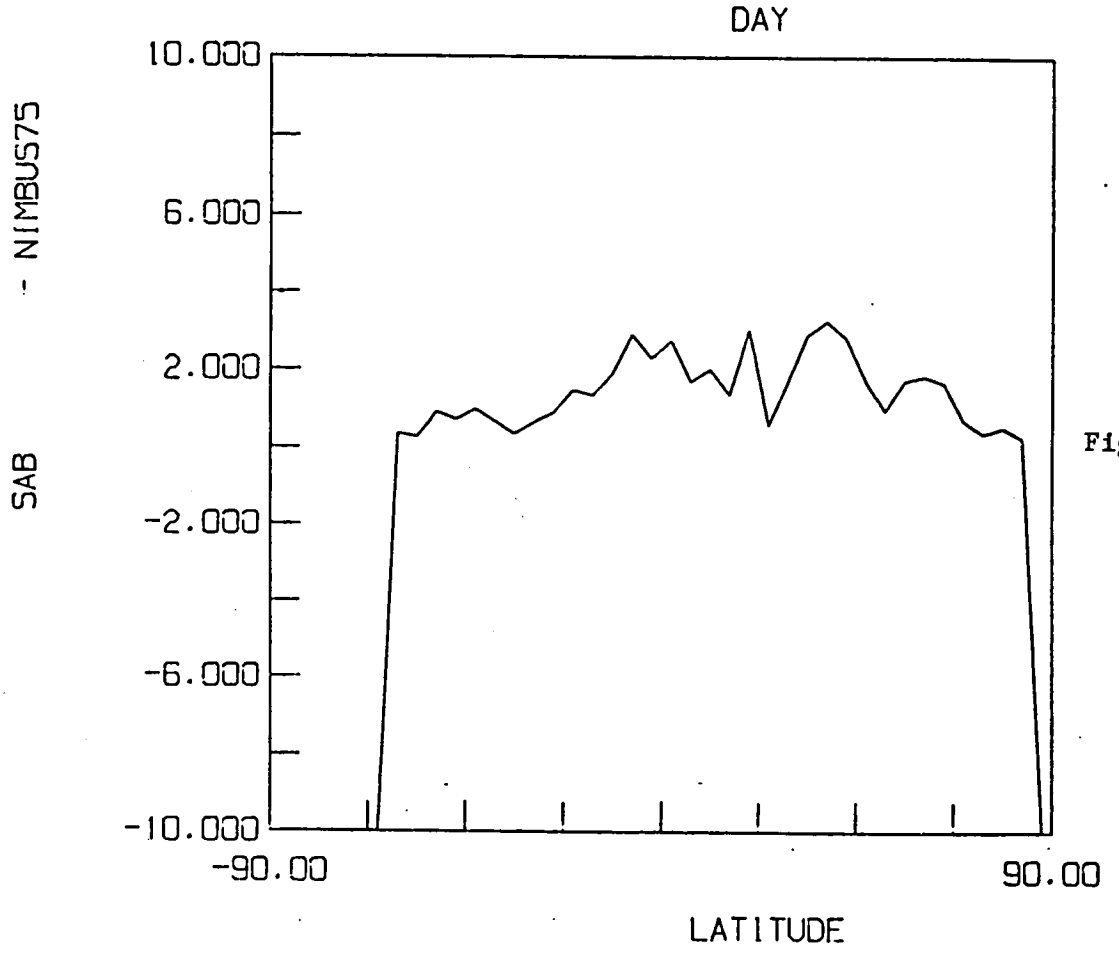

Figure 8a

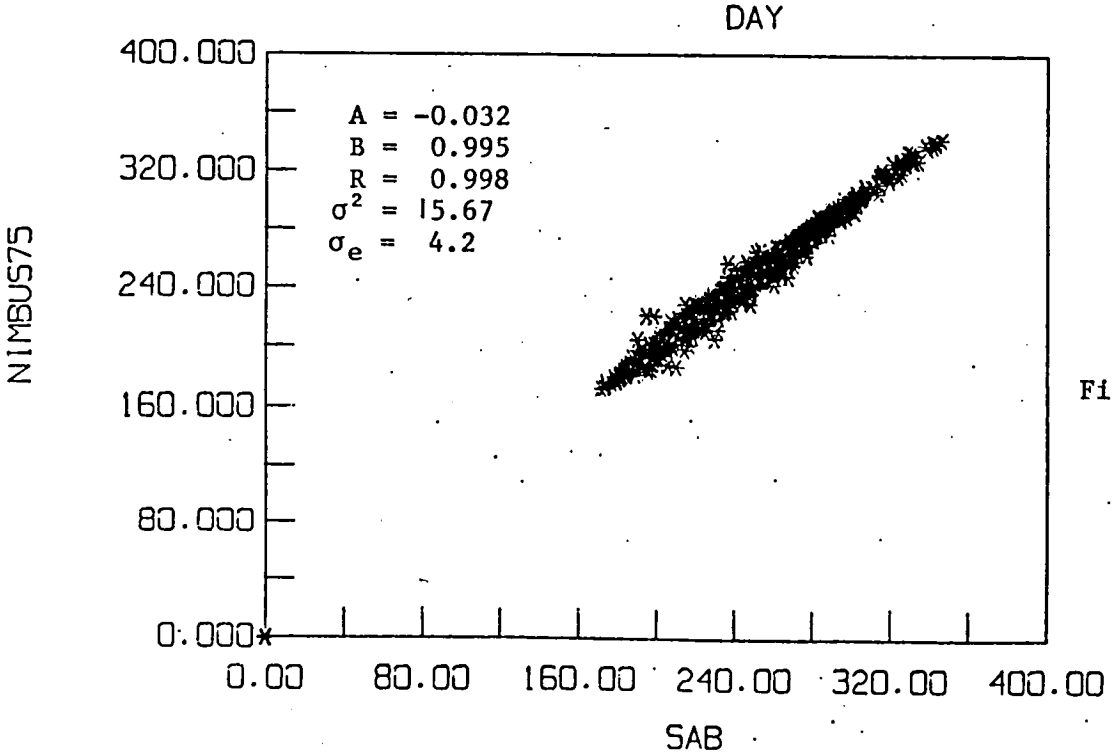

Figure 8b

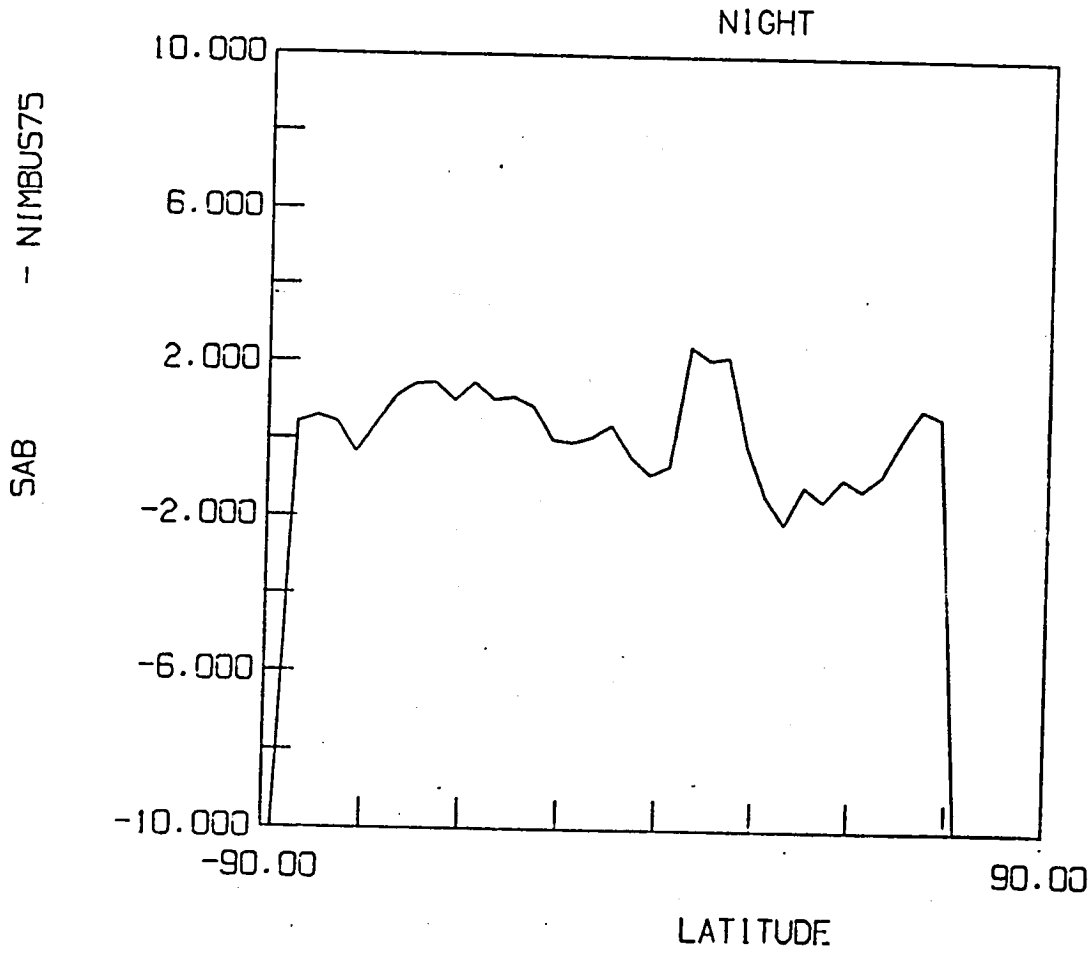

Figure 9a

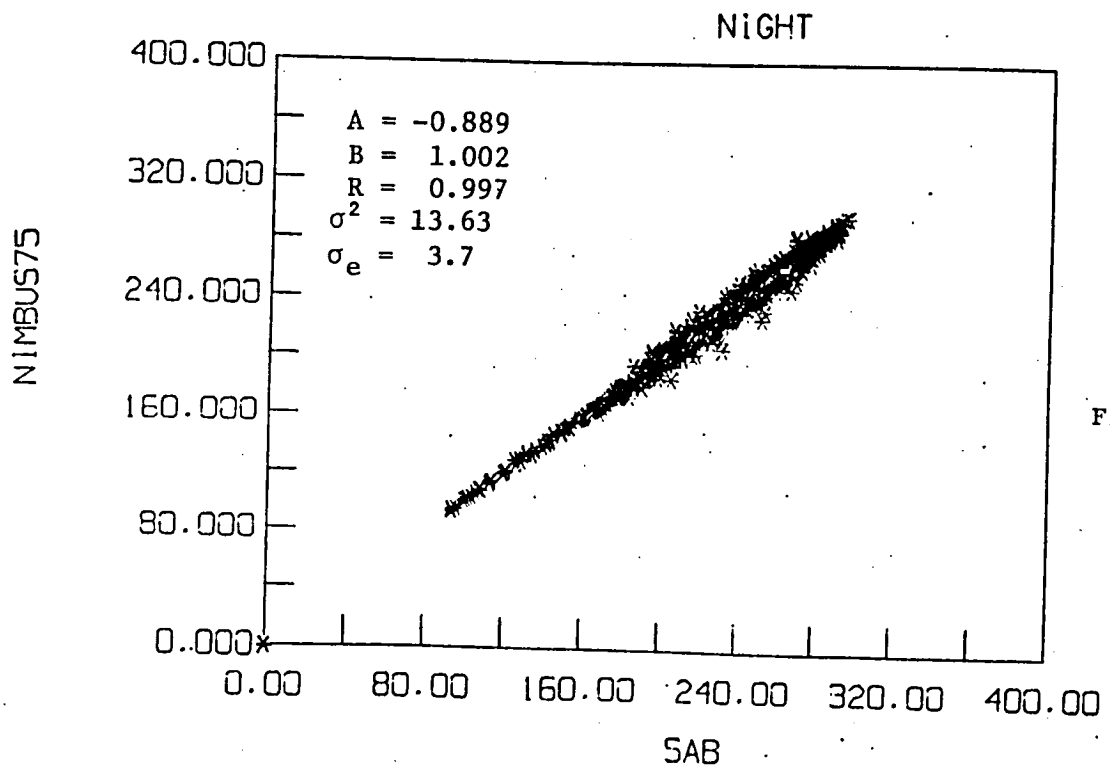

Figure 9b

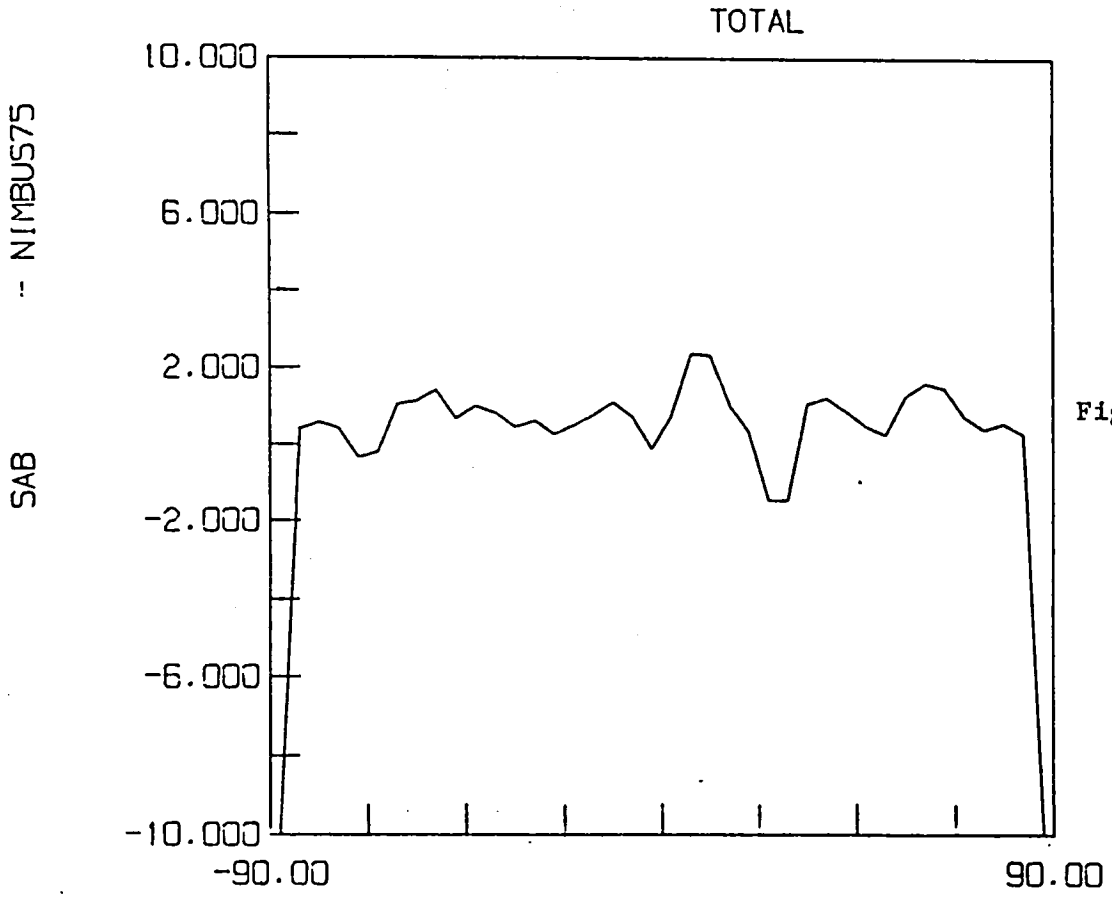

Figure 10a

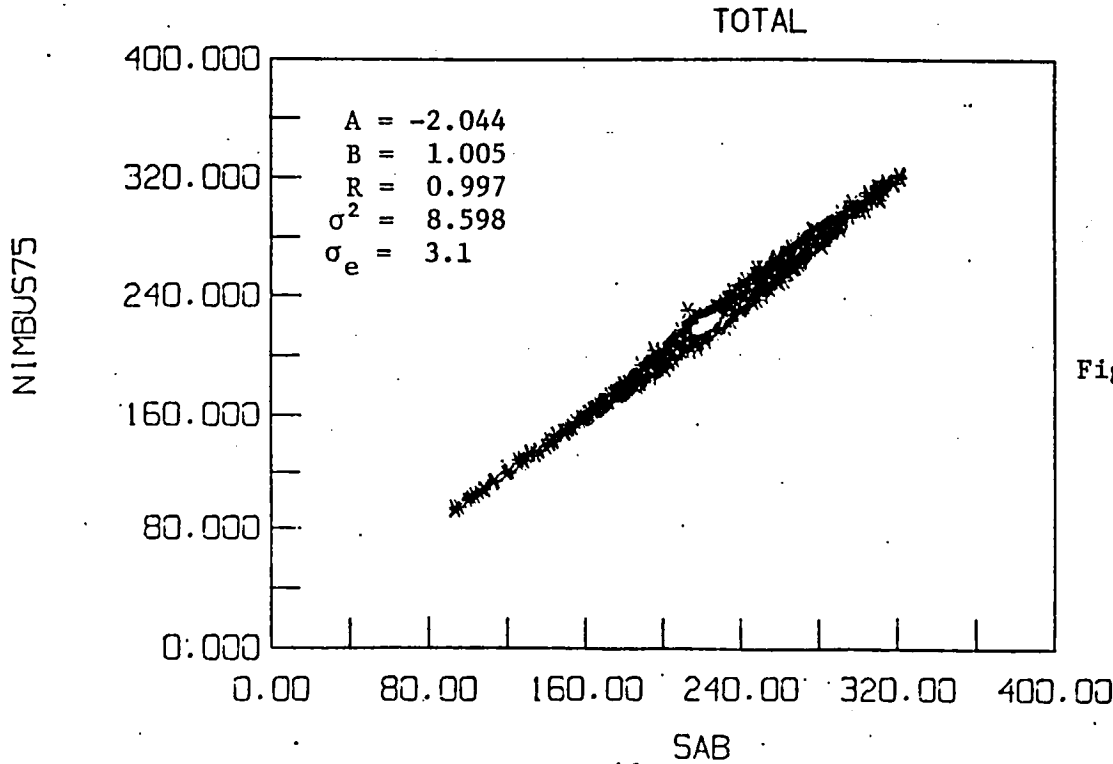

Figure 10b

Figure 11.

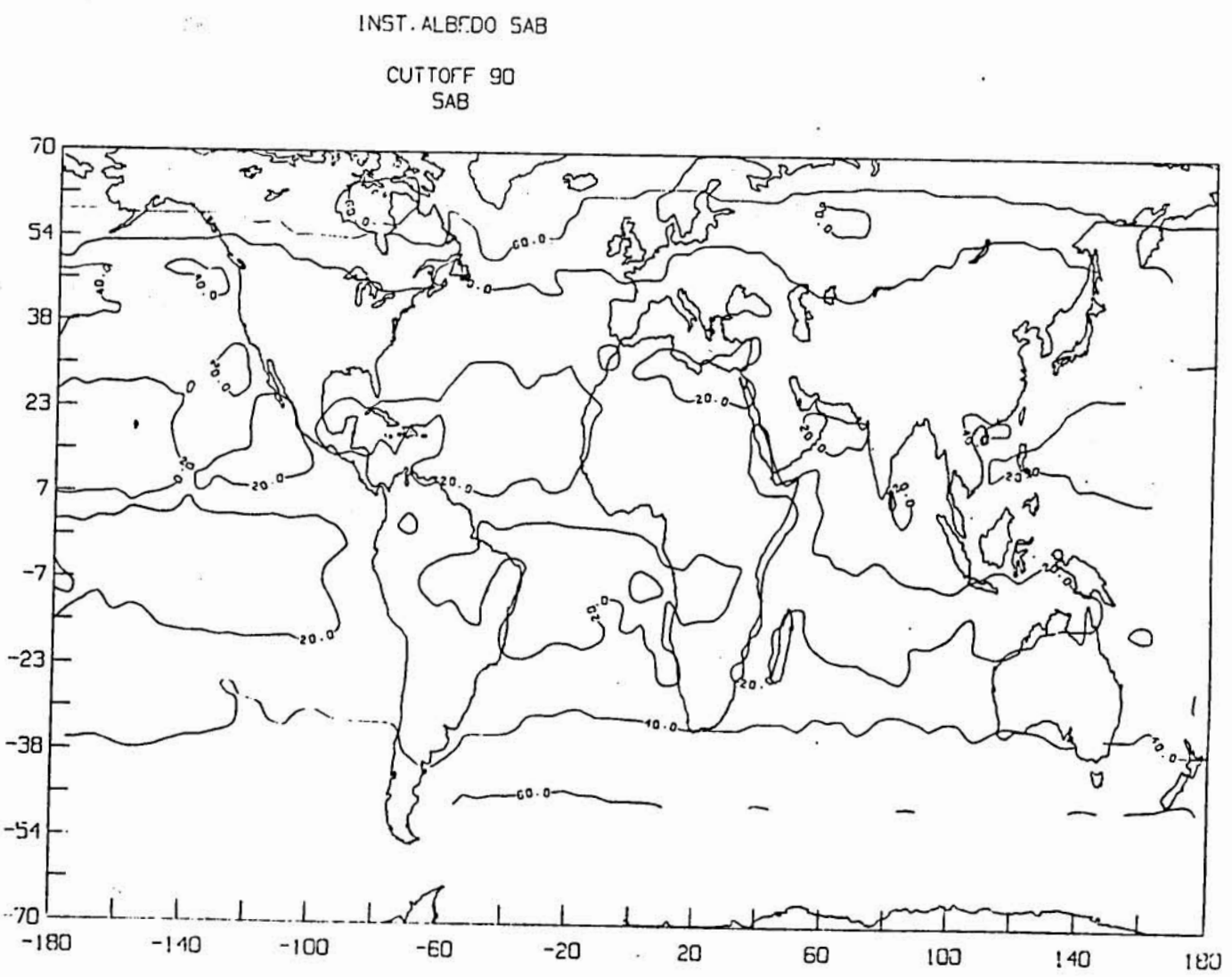
INST. ALBEDO SAB
CUTTOFF 90
SAB
70
54
38
23
7
-7
-23
-38
-54
-70
-180
-140
-100
-60
-20
20
60
100
140
180

Figure 12.

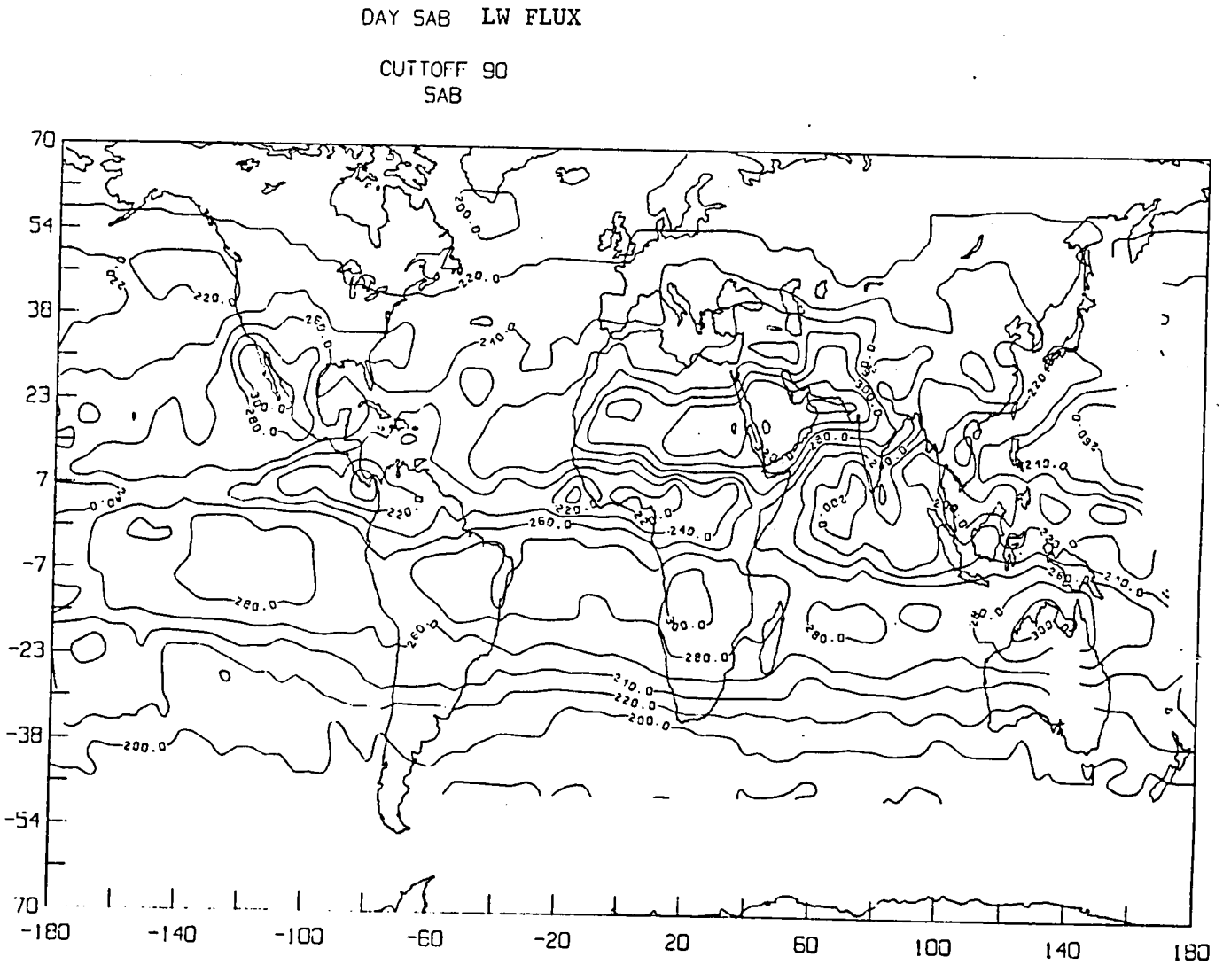
DAY SAB LW FLUX
CUTTOFF 90
SAB
70
54
38
23
7
-7
-23
-38
-54
-70
-180
-140
-100
-60
-20
20
60
100
140
180

Figure 13.

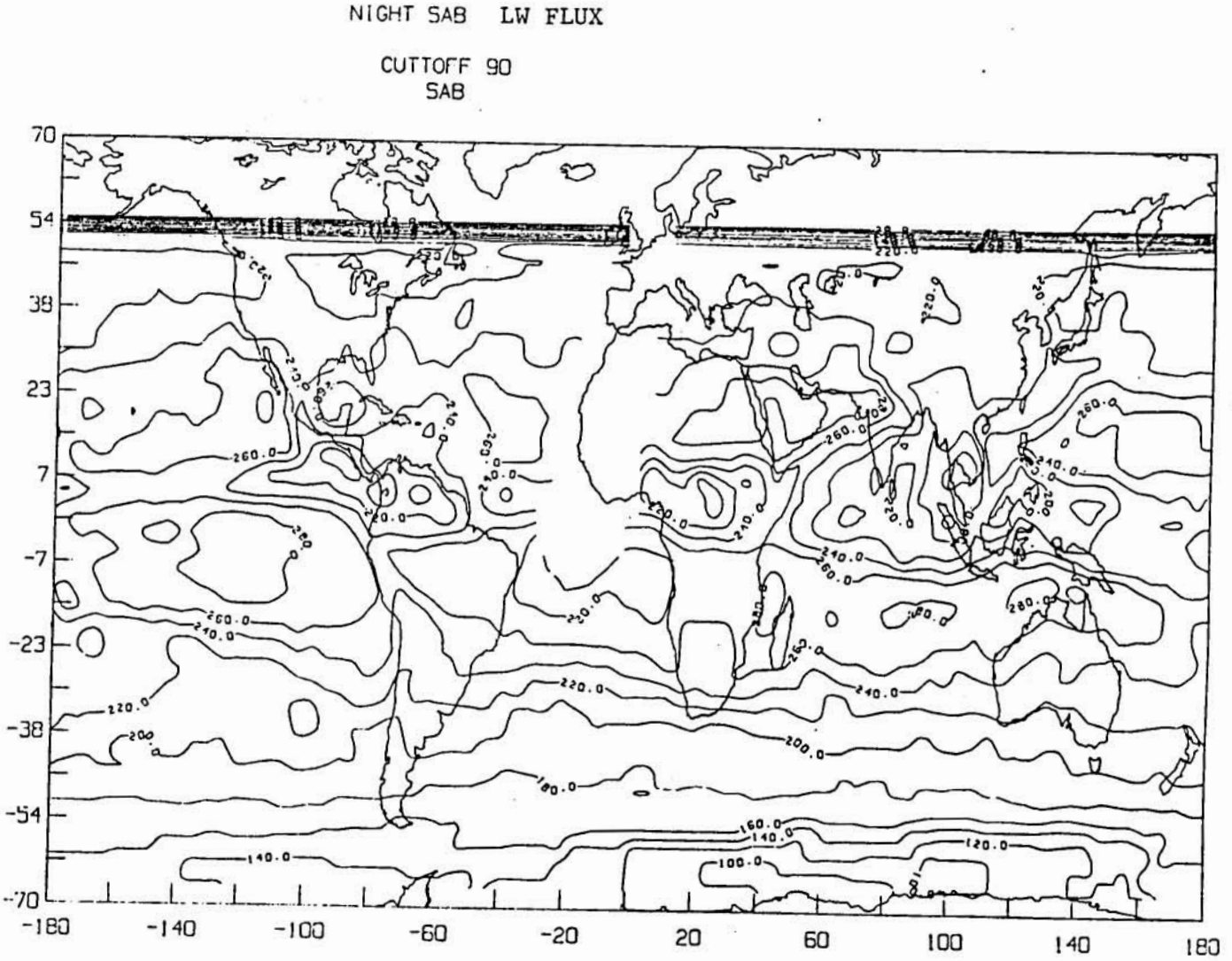
NIGHT SAB LW FLUX
CUTTOFF 90
SAB
70
54
38
23
7
-7
-23
-38
-54
-70
-180
-140
-100
-60
-20
20
60
100
140
180

Figure 14.

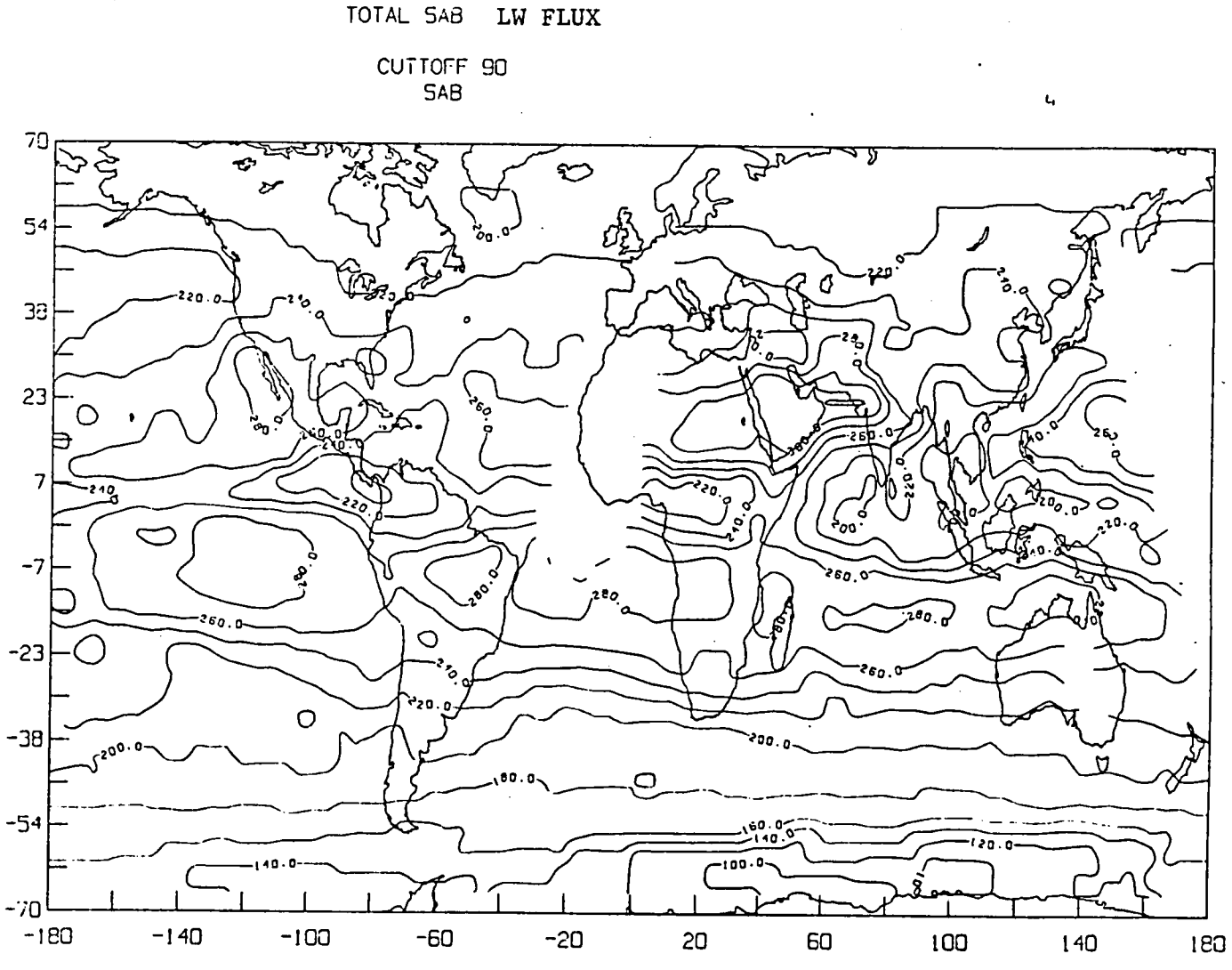
TOTAL SAB LW FLUX
CUTTOFF 90
SAB
70
54
38
23
7
-7
-23
-38
-54
-70
-180
-140
-100
-60
-20
20
60
100
140
180

Figure 15.

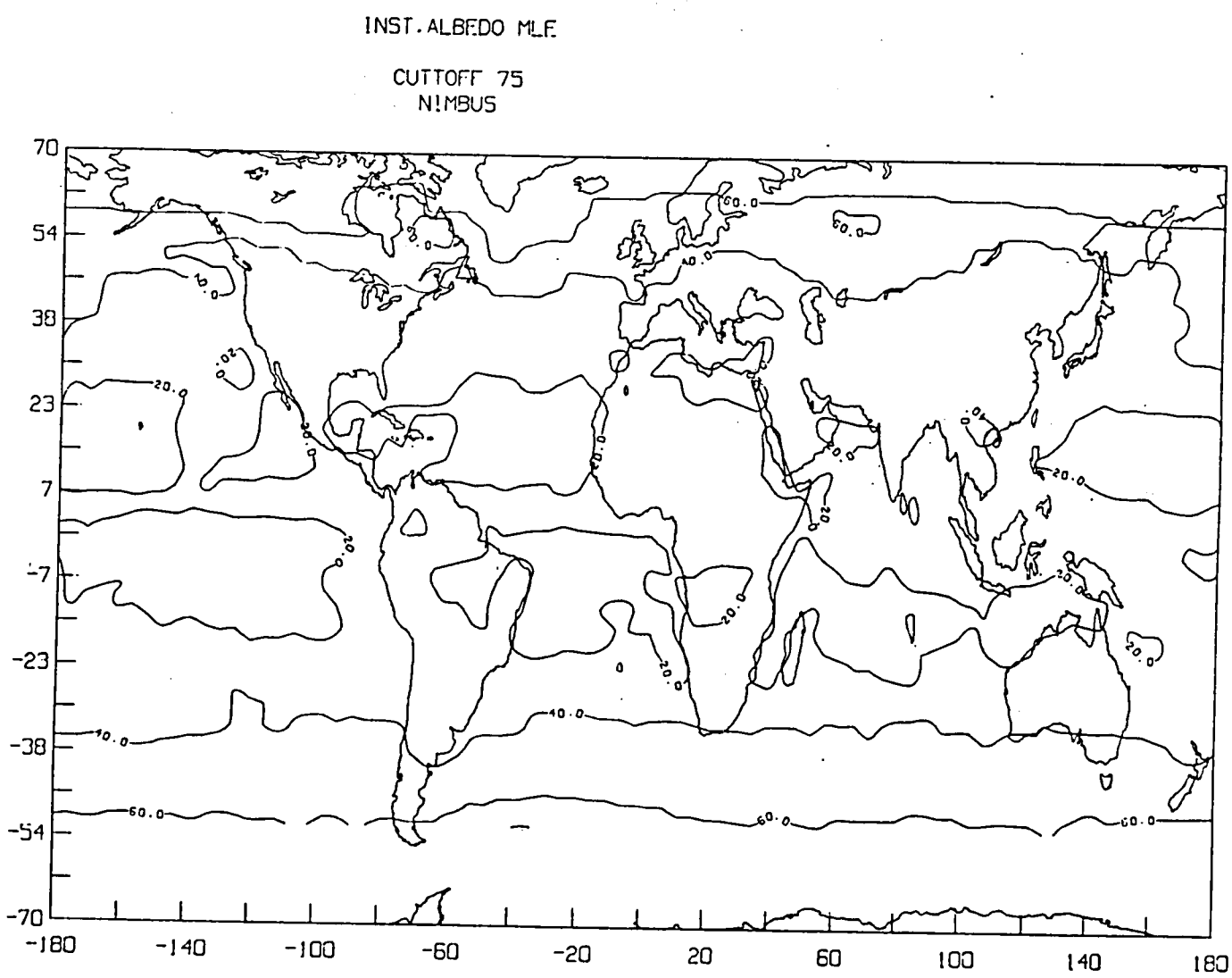
INST. ALBEDO MLE
CUTTOFF 75
NIMBUS
70
54
38
23
7
-7
-23
-38
-54
-70
-180
-140
-100
-60
-20
20
60
100
140
180

Figure 16.

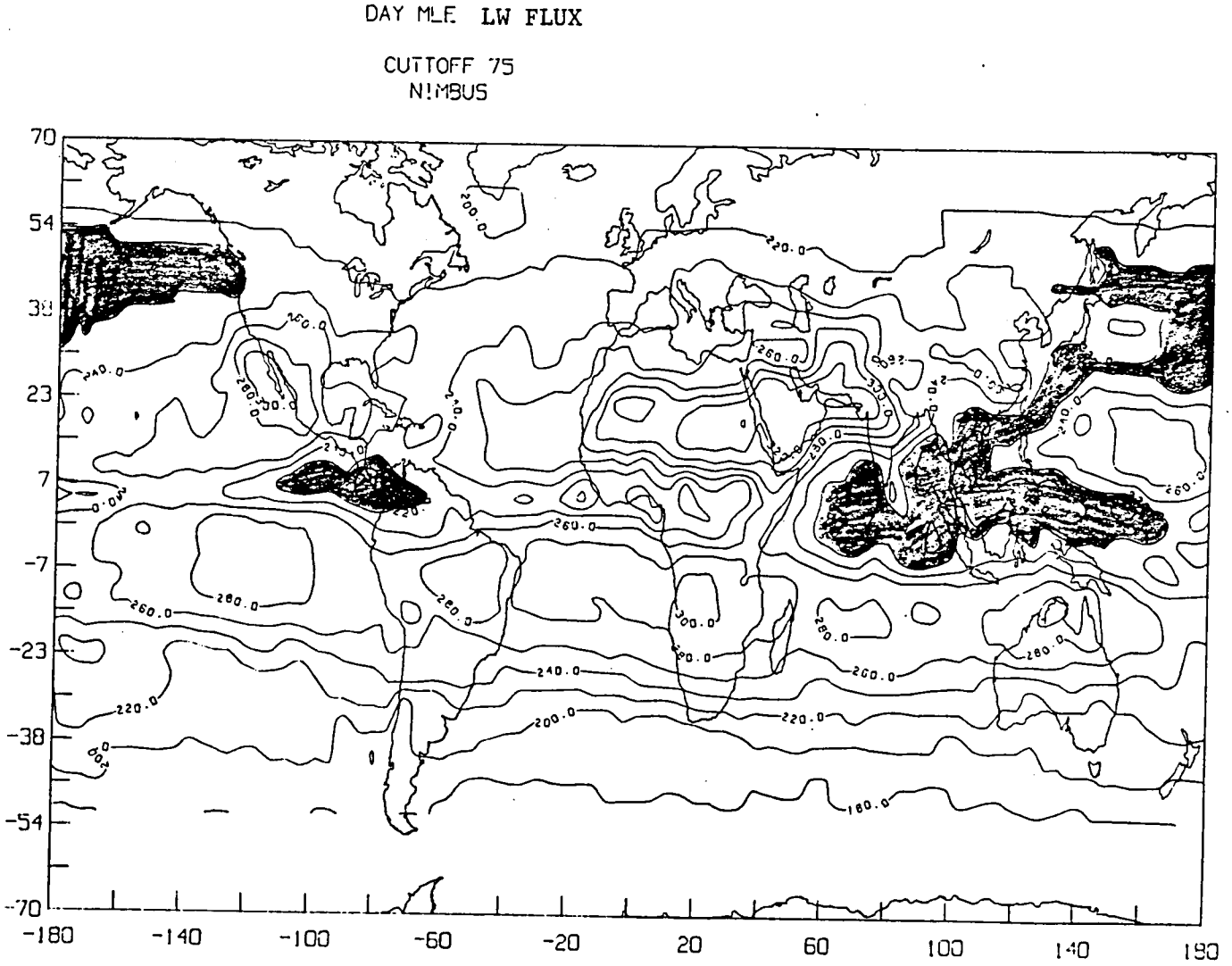
DAY MLE LW FLUX
CUTTOFF 75
NIMBUS
70
54
38
23
7
-7
-23
-38
-54
-70
-180
-140
-100
-60
-20
20
60
100
140
180

Figure 17.

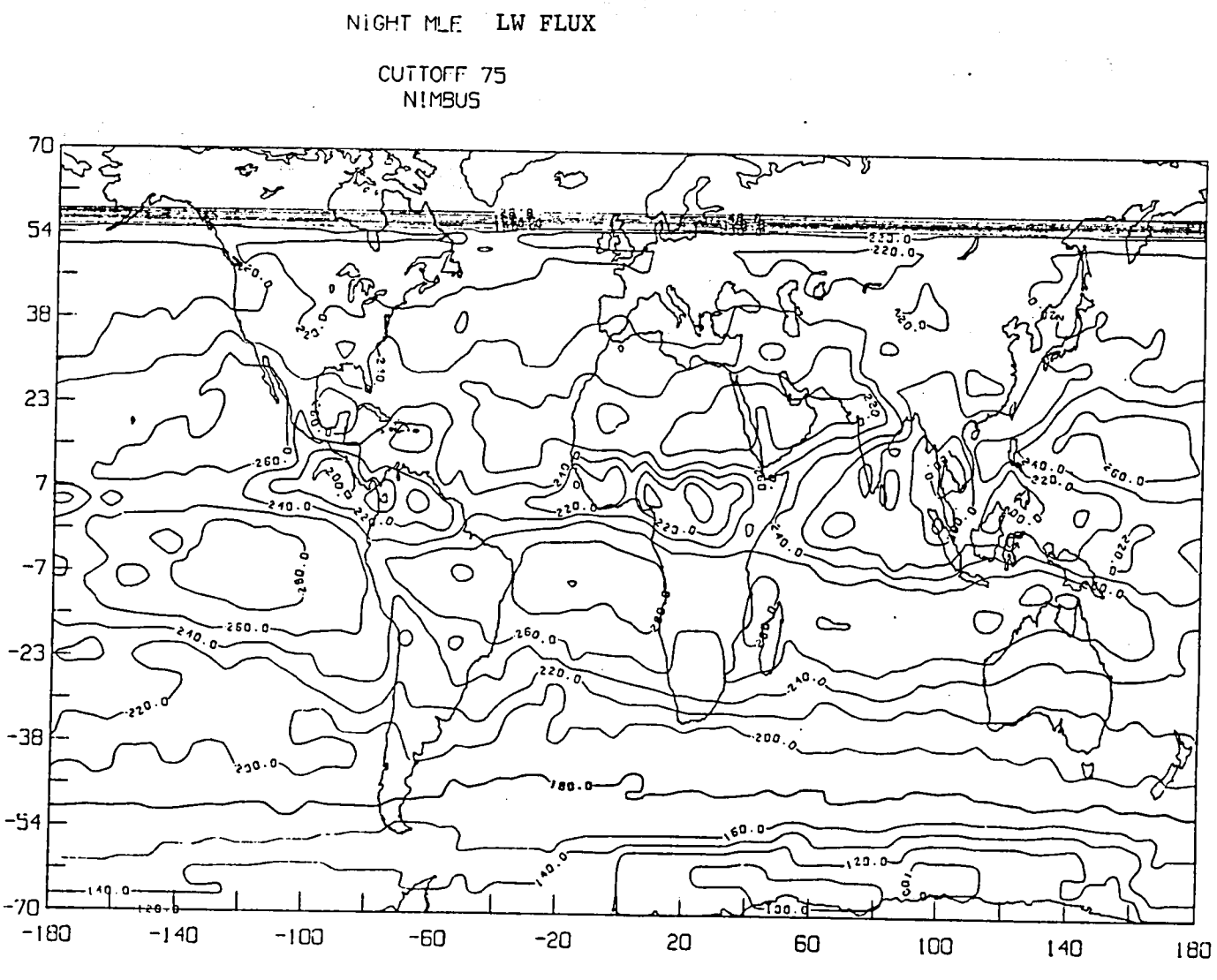
NIGHT MLE LW FLUX
CUTTOFF 75
NIMBUS
70
54
38
23
7
-7
-23
-38
-54
-70
-180
-140
-100
-60
-20
20
60
100
140
180

Figure 18.

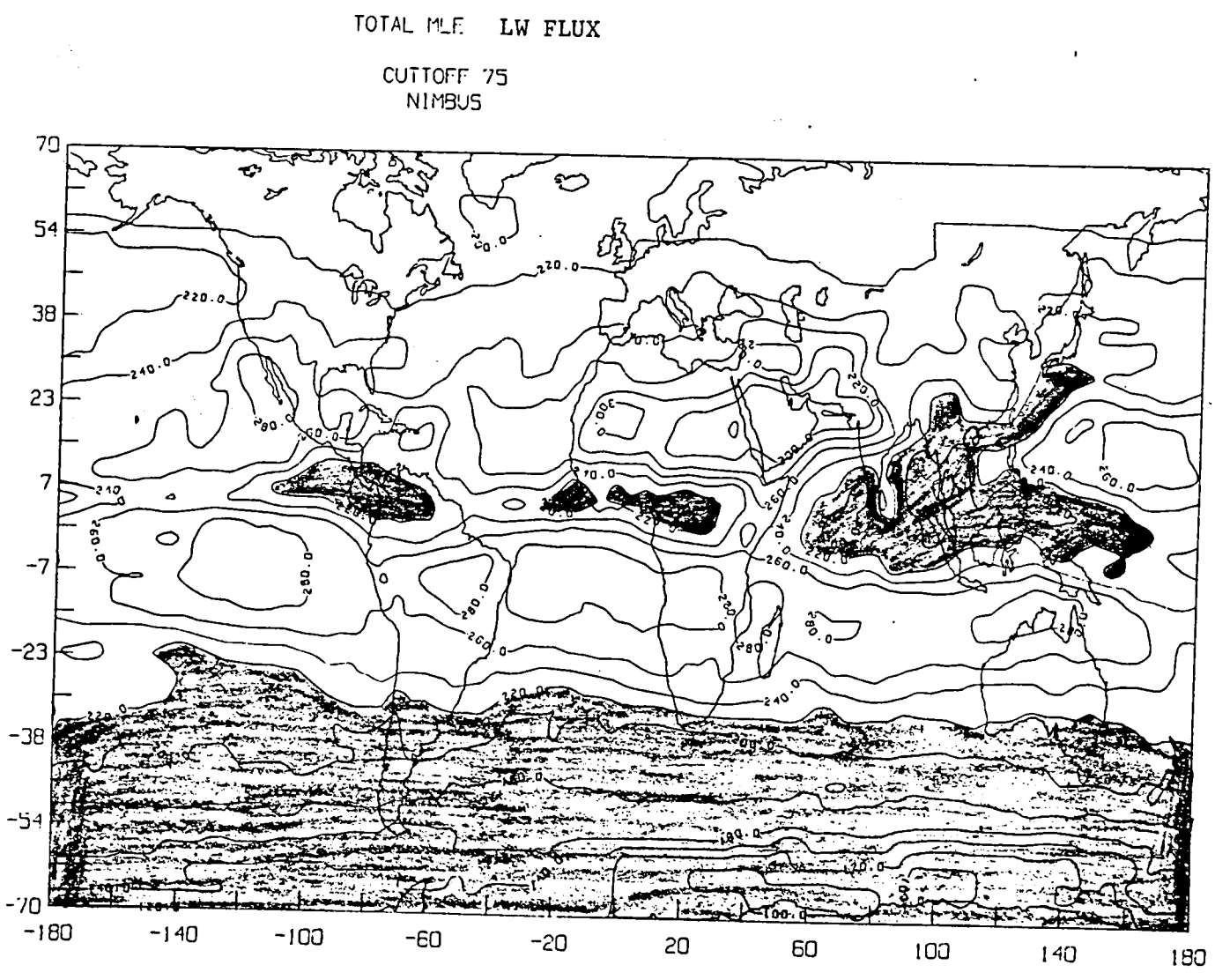
TOTAL MLE LW FLUX
CUTTOFF 75
NIMBUS
70
54
38
23
7
-7
-23
-38
-54
-70
-180
-140
-100
-60
-20
20
60
100
140
180

Figure 19.

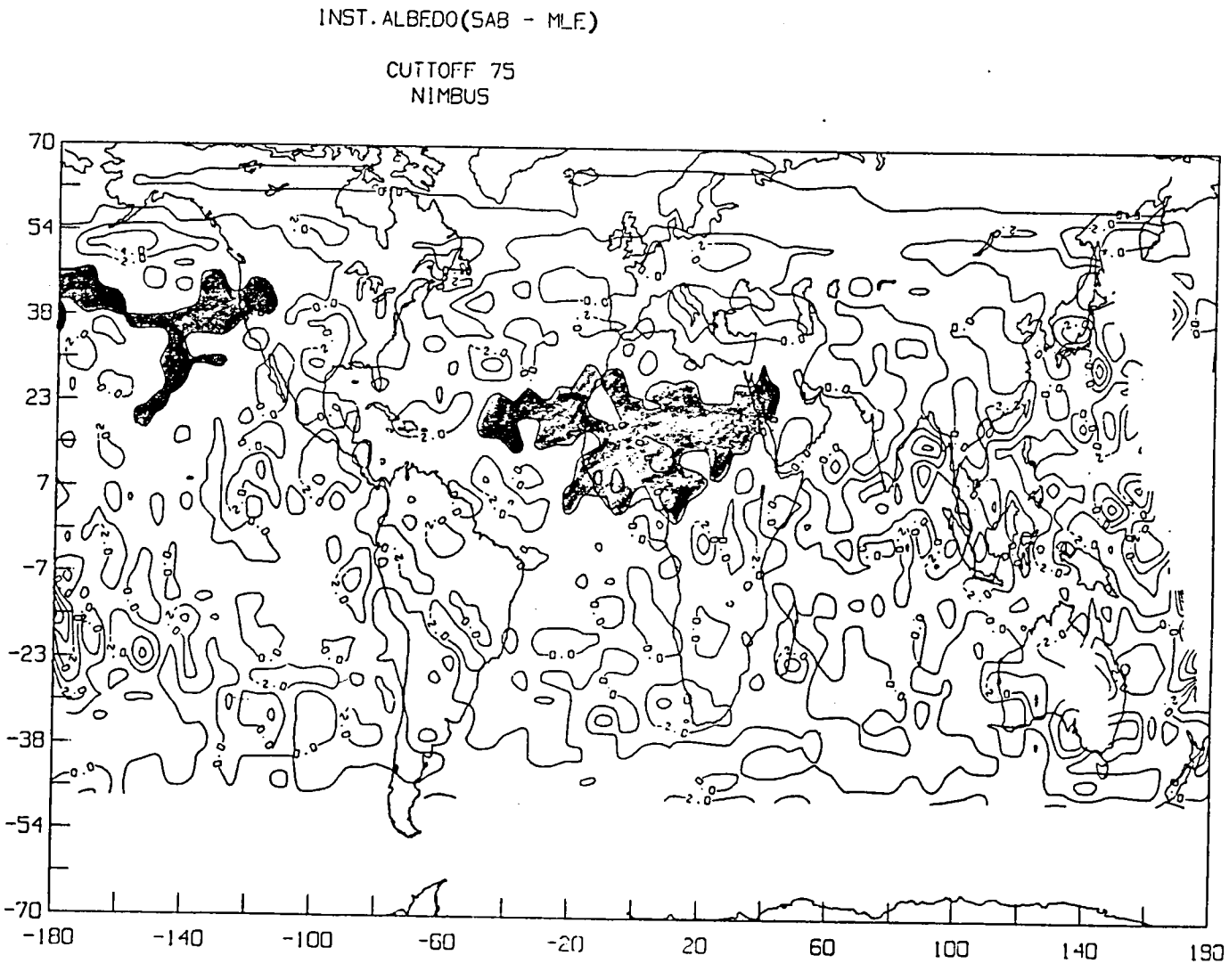
INST. ALBEDO(SAB - MLE)
CUTOFF 75
NIMBUS
70
54
38
23
7
-7
-23
-38
-54
-70
-180
-140
-100
-60
-20
20
60
100
140
180

Figure 20.

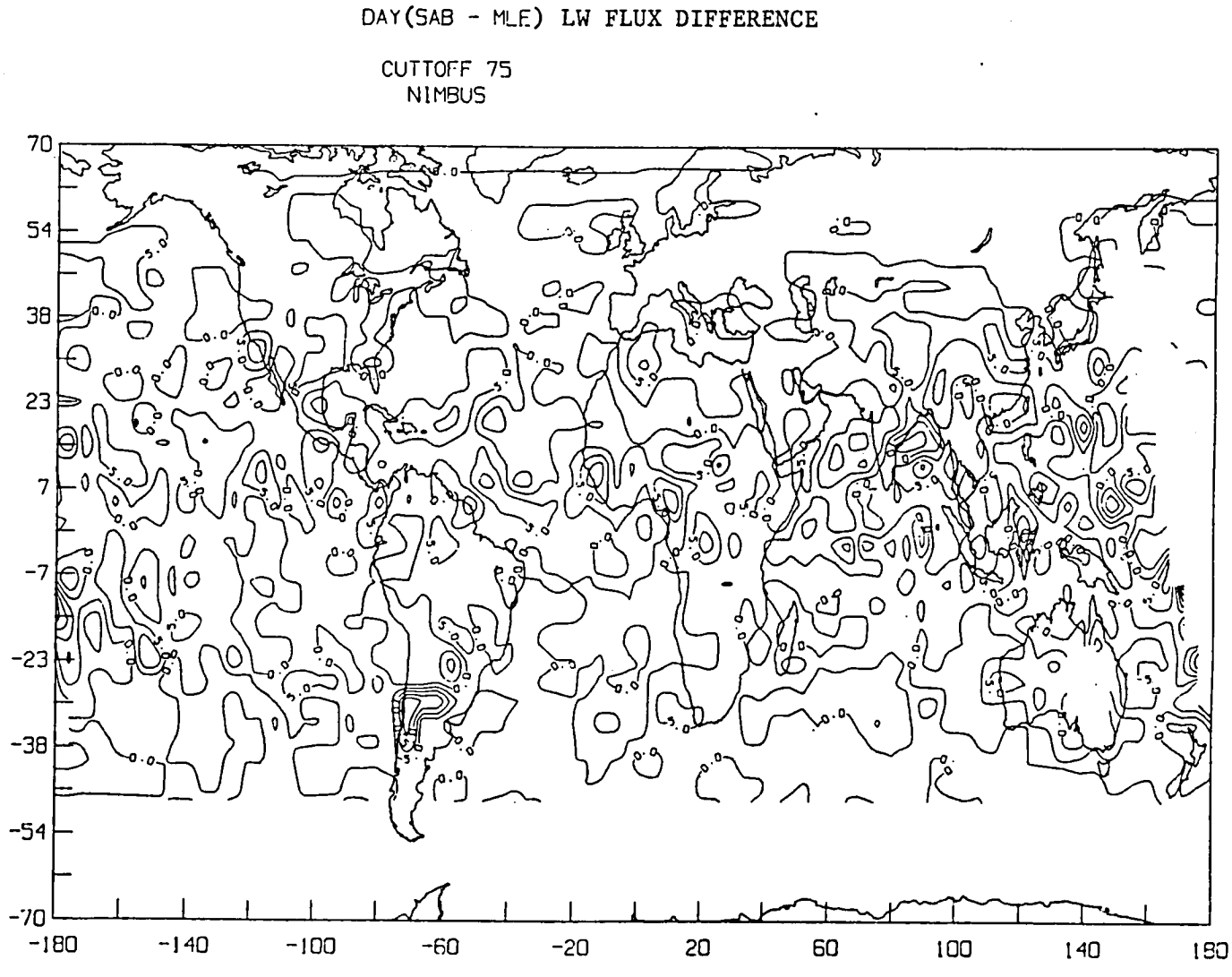
DAY(SAB - MLE) LW FLUX DIFFERENCE
CUTTOFF 75
NIMBUS
70
54
38
23
7
-7
-23
-38
-54
-70
-180
-140
-100
-60
-20
20
60
100
140
180

Figure 21.

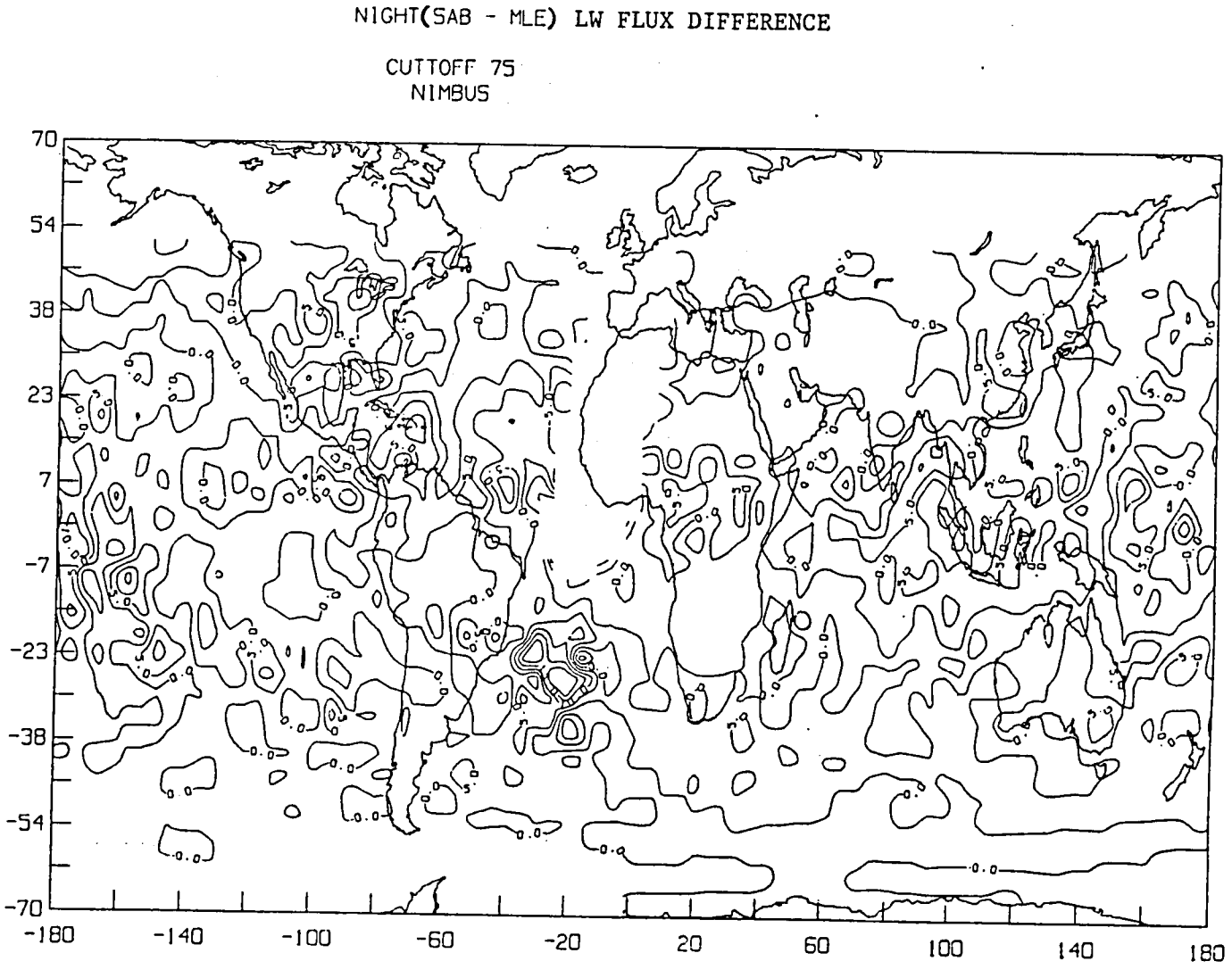
NIGHT(SAB - MLE) LW FLUX DIFFERENCE
CUTTOFF 75
NIMBUS
70
54
38
23
7
-7
-23
-38
-54
-70
-180
-140
-100
-60
-20
20
60
100
140
180
0.0

Figure 22.

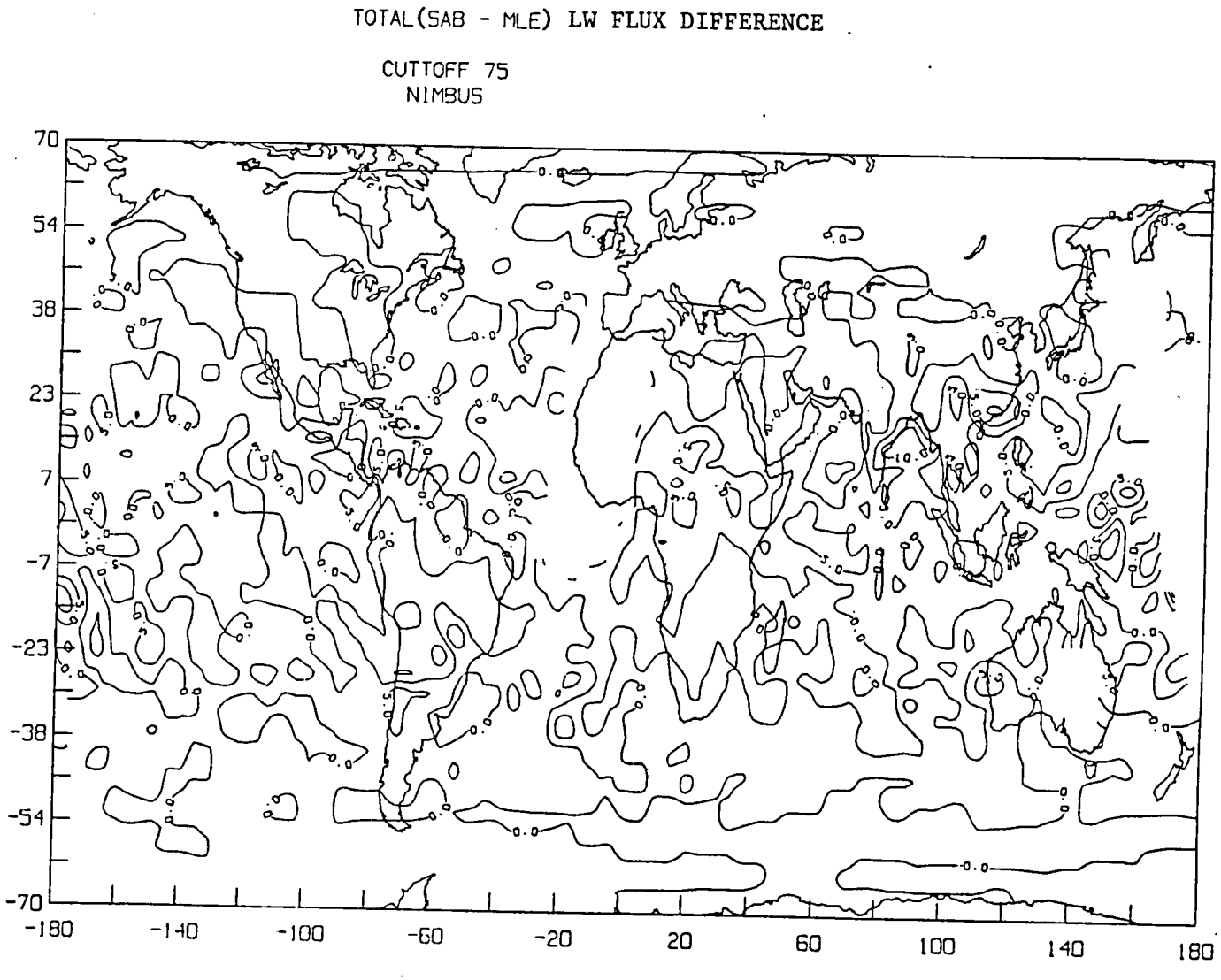
TOTAL(SAB - MLE) LW FLUX DIFFERENCE
CUTTOFF 75
NIMBUS
70
54
38
23
7
-7
-23
-38
-54
-70
-180
-140
-100
-60
-20
20
60
100
140
180

Figure 23.

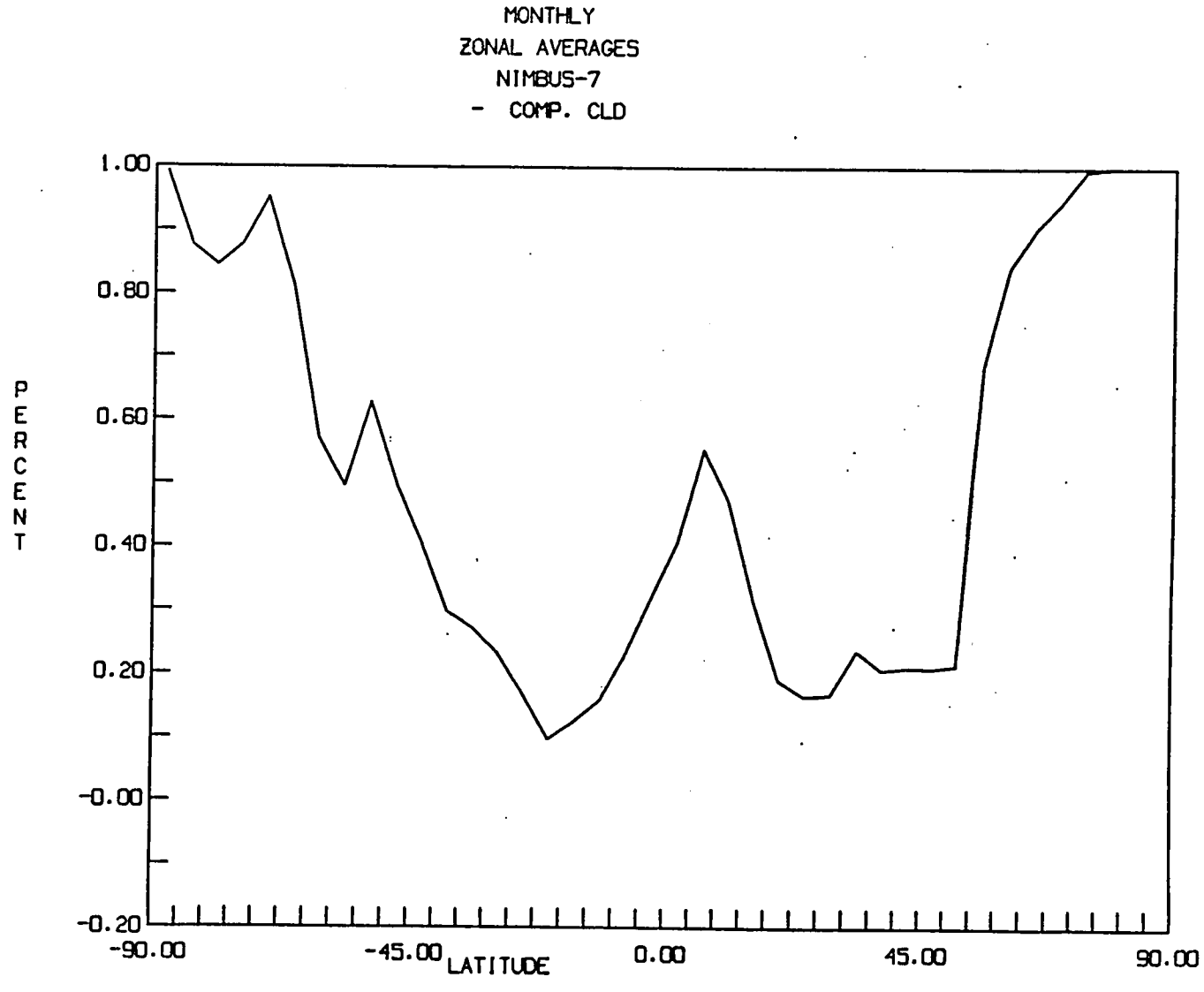
MONTHLY
ZONAL AVERAGES
NIMBUS-7
- COMP. CLD
1.00
0.80
0.60
0.40
0.20
-0.00
-0.20
PERCENT
-90.00
-45.00
LATITUDE
0.00
45.00
90.00

Figure 24.

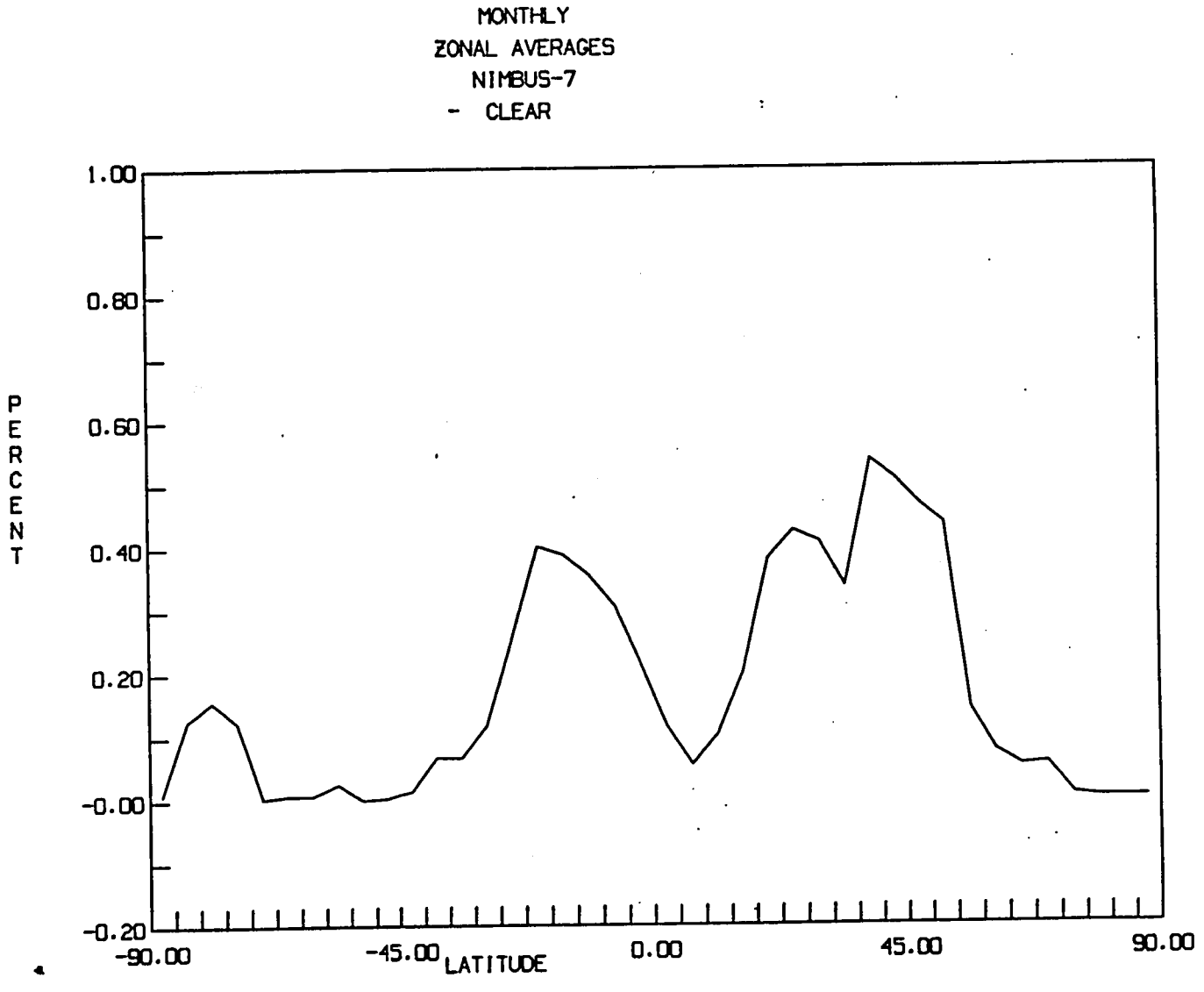
MONTHLY
ZONAL AVERAGES
NIMBUS-7
- CLEAR
1.00
0.80
0.60
0.40
0.20
-0.00
-0.20
PERCENT
-90.00
-45.00
0.00
45.00
90.00
LATITUDE

Figure 25.

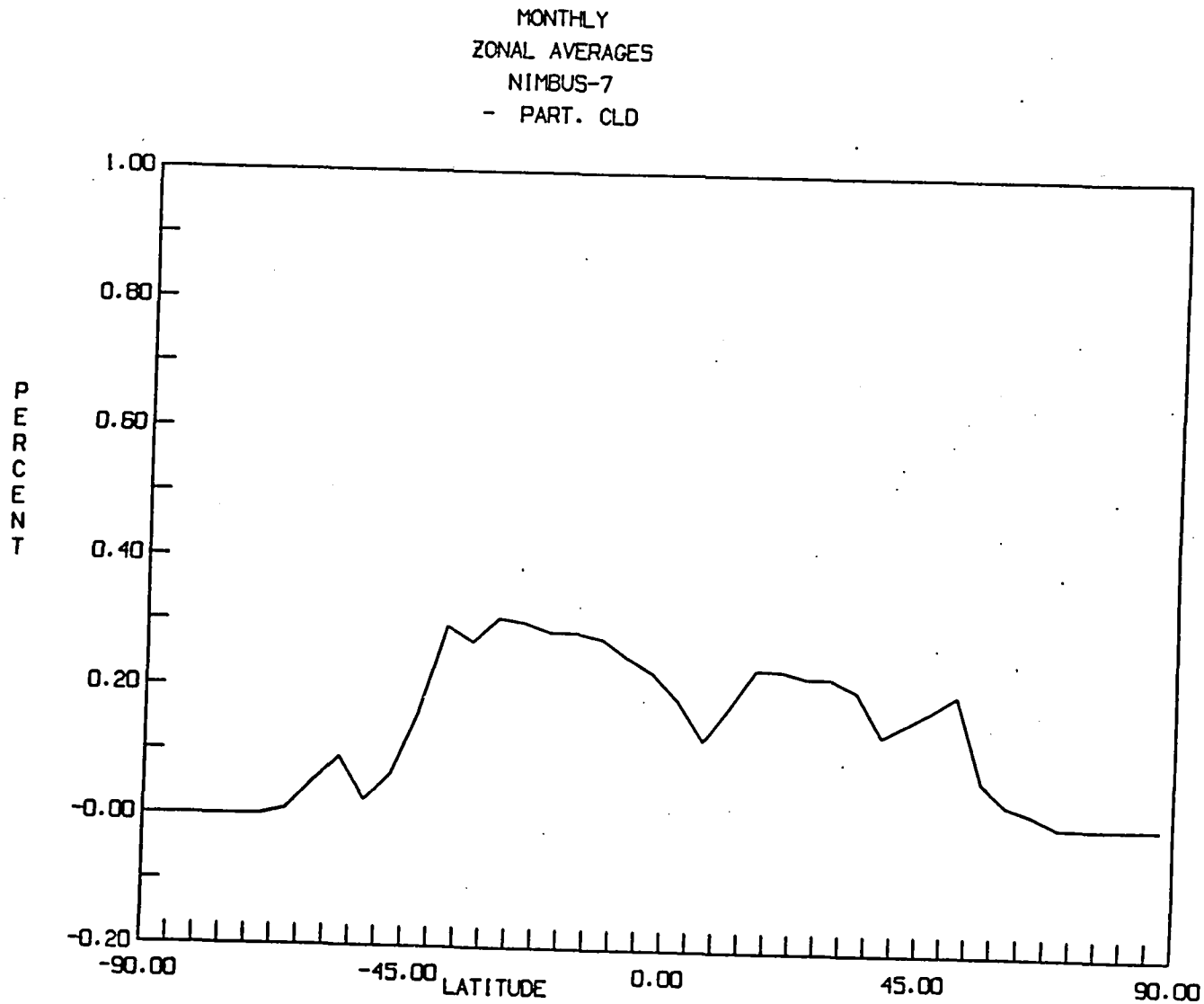
MONTHLY
ZONAL AVERAGES
NIMBUS-7
- PART. CLD
1.00
0.80
0.60
0.40
0.20
-0.00
-0.20
PERCENT
-90.00
-45.00
LATITUDE
0.00
45.00
90.00

Figure 26.

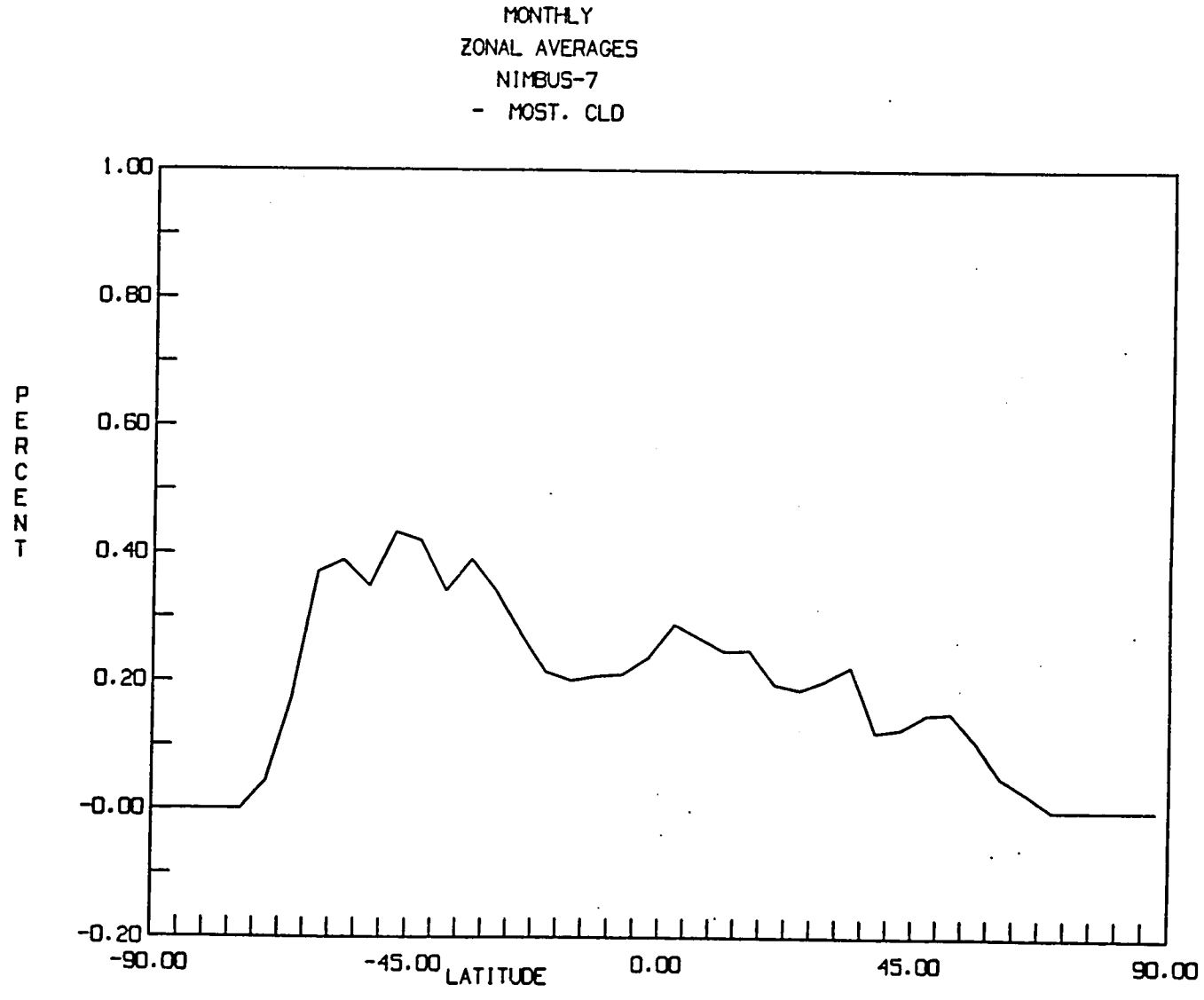
MONTHLY
ZONAL AVERAGES
NIMBUS-7
- MOST. CLD
1.00
0.80
0.60
0.40
0.20
-0.00
-0.20
PERCENT
-90.00
-45.00
LATITUDE
0.00
45.00
90.00

Figure 27.

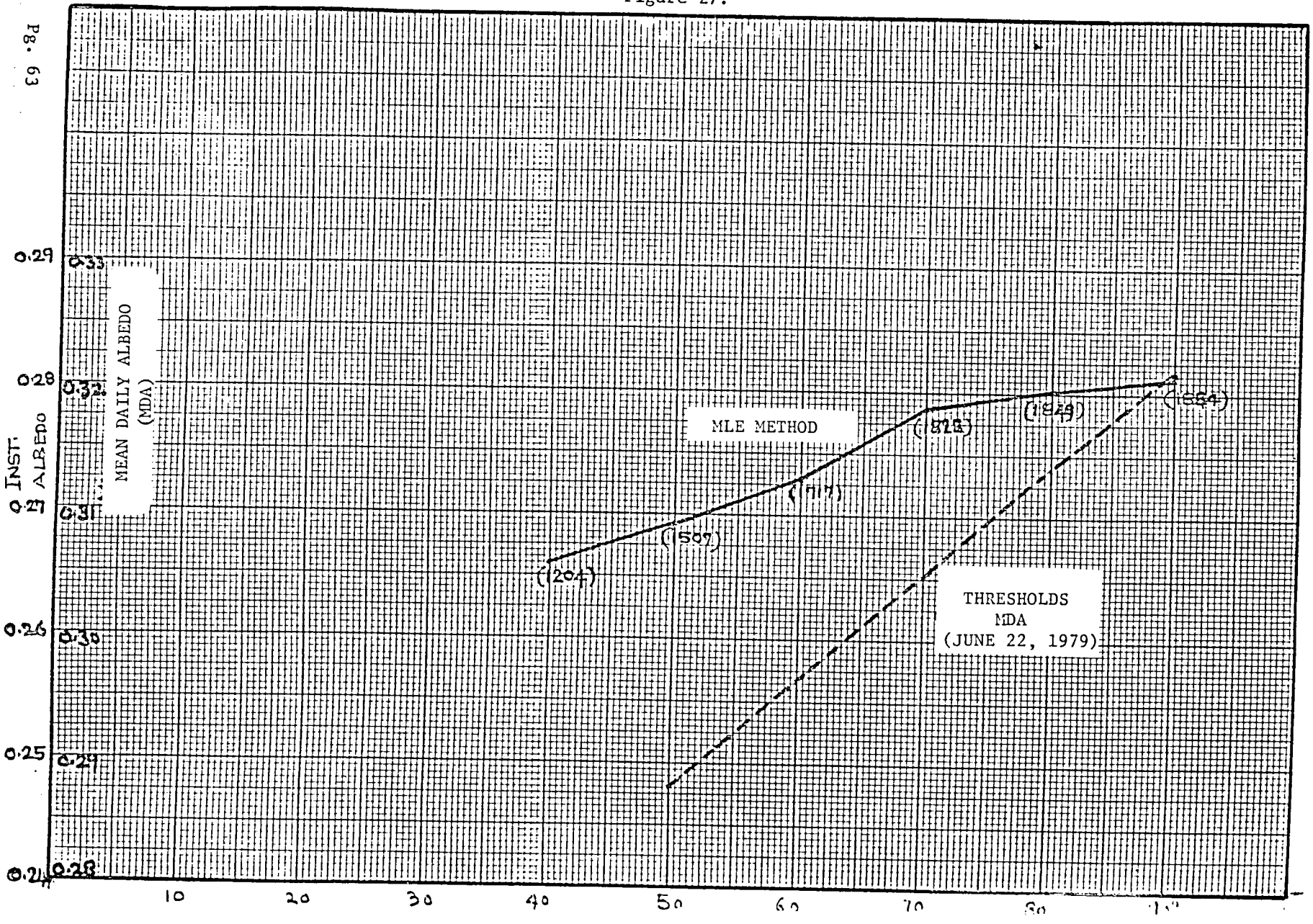
INST. ALBEDO
MEAN DAILY ALBEDO (MDA)
MLE METHOD
THRESHOLDS MDA (JUNE 22, 1979)
0.29
0.28
0.27
0.26
0.25
0.24
0.33
0.32
0.31
0.30
0.29
0.28
(204)
(507)
(717)
(872)
(849)
(654)
10
20
30
40
50
60
70
80

Figure 28.

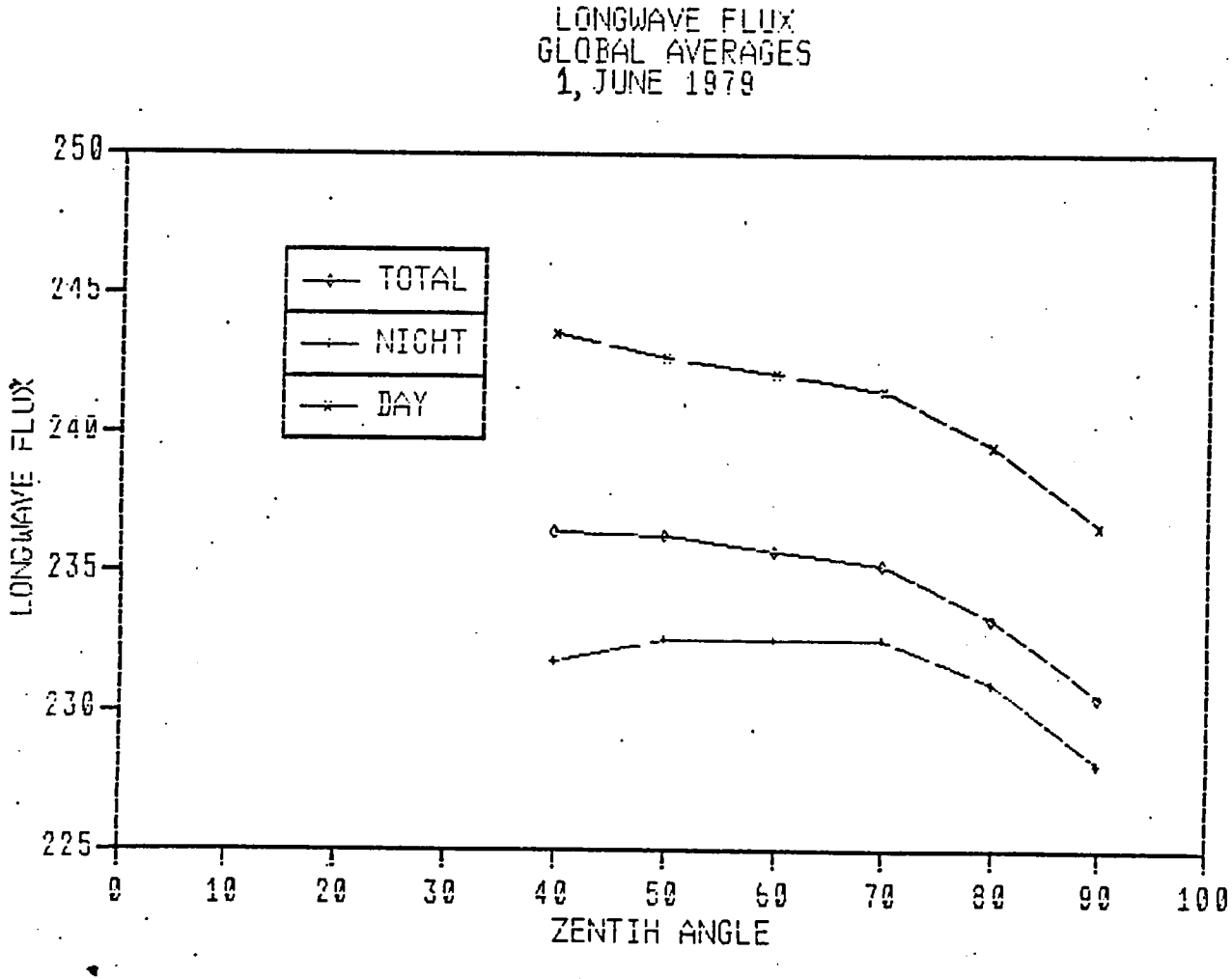
LONGWAVE FLUX
GLOBAL AVERAGES
1, JUNE 1979
TOTAL
NIGHT
DAY
LONGWAVE FLUX
250
245
240
235
230
225
0
10
20
30
40
50
60
70
80
90
100
ZENTIH ANGLE

Figure 29.

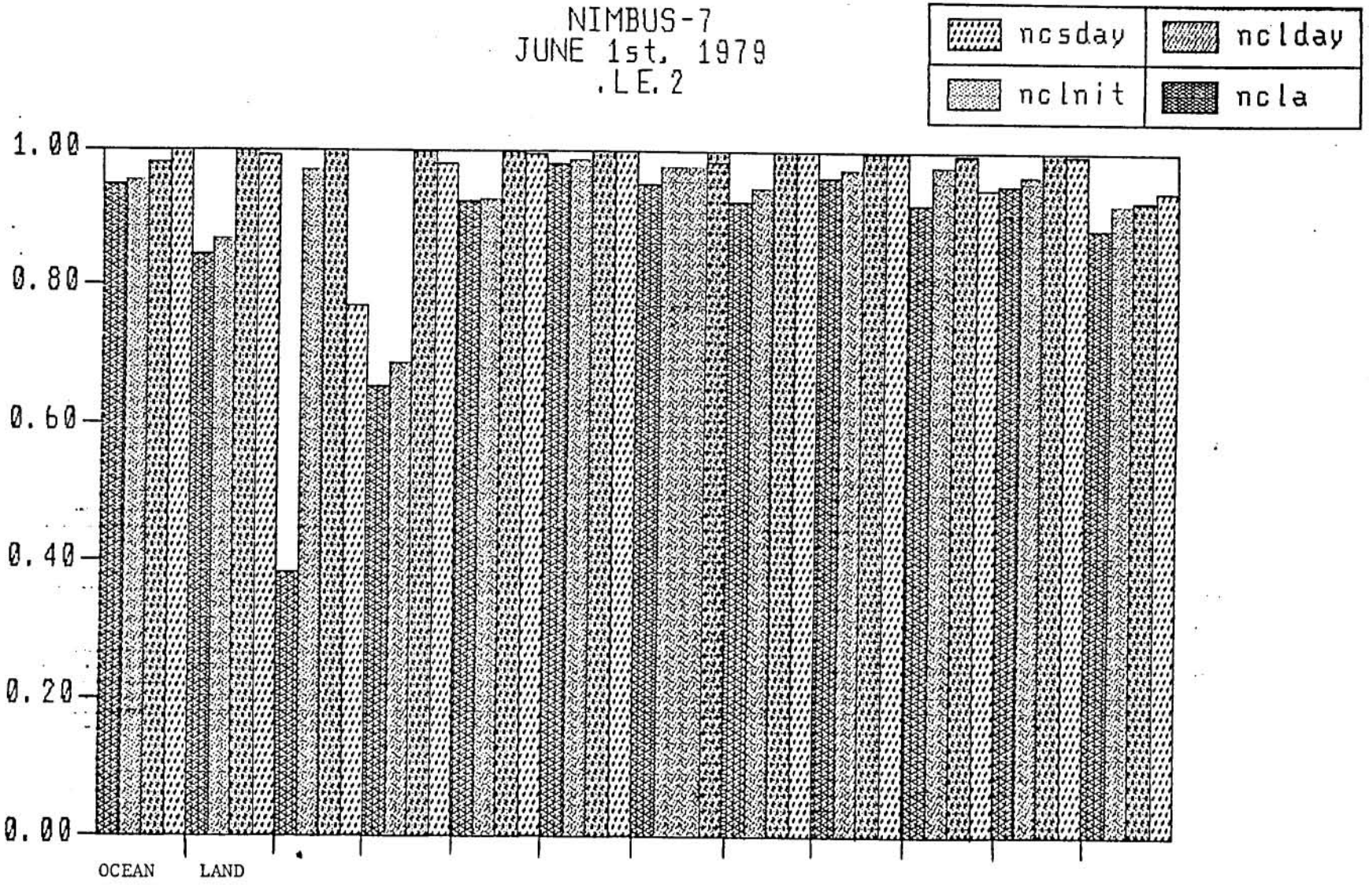
NIMBUS-7
JUNE 1st, 1979
.L E. 2
ncsday
nclday
nclnit
ncla
1.00
0.80
0.60
0.40
0.20
0.00
OCEAN
LAND

Figure 30.

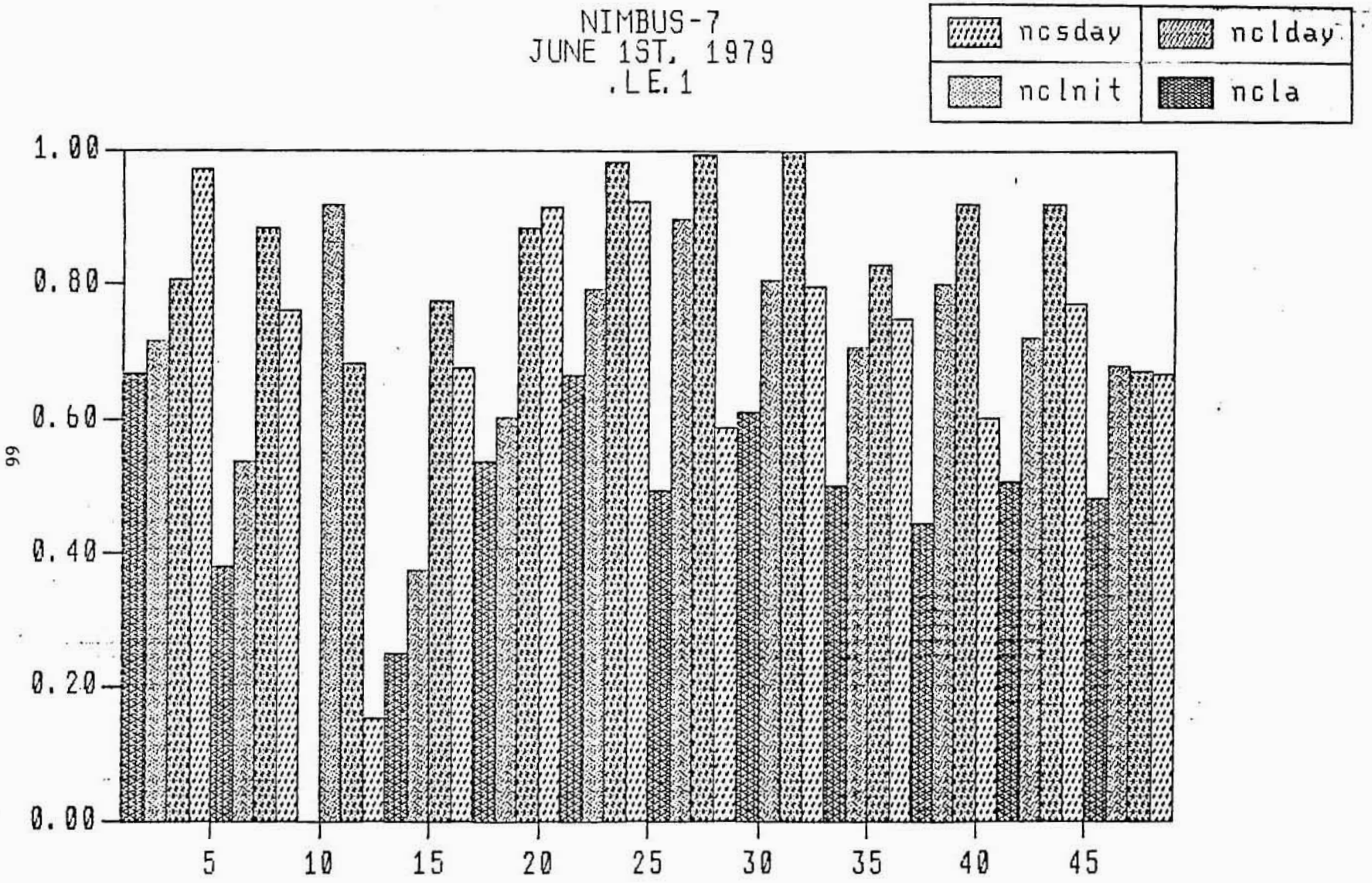
NIMBUS-7
JUNE 1ST, 1979
.LE.1
ncsday
nclday
nclnit
ncla
1.00
0.80
0.60
0.40
0.20
0.00
99
5
10
15
20
25
30
35
40
45

1. Report No.	2. Government Accession No.	3. Recipient's Catalog No.
NASA CR-172596		

4. Title and Subtitle	5. Report Date
VALIDATION OF THE ERBE SCANNER SCENE IDENTIFICATION METHODOLOGY: ANALYSIS WITH NIMBUS-7ERB DATA	March 1985
	6. Performing Organization Code

7. Author(s)	8. Performing Organization Report No.
Sastri Vermury	SMSRC DOC. NO. 7-85
	10. Work Unit No.

9. Performing Organization Name and Address	11. Contract or Grant No.
S M Systems and Research Corporation 8401 Corporate Drive, Suite 450 Landover, MD 20785	L-67978B
	13. Type of Report and Period Covered
12. Sponsoring Agency Name and Address	Contractor Report
National Aeronautics and Space Administration Washington, DC 20546	14. Sponsoring Agency Code
	619-12-30-01

15. Supplementary Notes

Langley Technical Monitor: John T. Suttles
Final Report

16. Abstract

Maximum Likelihood Estimation (MLE) procedure for scene identification currently being utilized in the ERBE scanner data processing stream is applied to the Nimbus-7 ERB Scanner data for the month of June 1979. The Earth radiation budget parameters derived using MLE method show very good agreement with the values provided using sorting into angular bins (SAB) method. Results of the fields on different spatial scales are presented. A satellite zenith angle study indicates that the MLE procedure considerably improves the scene selection over the method of bispectral thresholds applied in the Nimbus-7 ERB data processing. Agreement with SAB results improved further when the observations were cut off at 75° in satellite zenith. Sampling constraints, however, require that the cut-off angle should not be lower than 70°. Quantitative details about the reliability of the scene identification are also presented.

17. Key Words (Suggested by Author(s))	18. Distribution Statement
Earth Radiation Budget Satellite Data Analysis Scene Identification Maximum Likelihood Estimation	Unclassified--Unlimited Subject Category 47

19. Security Classif. (of this report)	20. Security Classif. (of this page)	21. No. of Pages	22. Price
Unclassified	Unclassified	68	A04

For sale by the National Technical Information Service, Springfield, Virginia 22161

DO NOT REMOVE SLIP FROM MATERIAL

Delete your name from this slip when returning material to the library.

NAME	DATE	MS
Patricia Hunter	4/10/96	197

NASA Langley (Rev. Dec. 1991) RIAD N-75